Quaternary Science Reviews 209 (2019) 82–99

Contents lists available at ScienceDirect

Quaternary Science Reviews

journal homepage: www.elsevier.com/locate/quascirev

Impact of Middle Pleistocene (Saalian) glacial lake-outburst floods on the meltwater-drainage pathways in northern central Europe: Insights from 2D numerical flood simulation

Jörg Lang [a, *], Petteri Alho [b, c], Elina Kasvi [b], Nils Goseberg [d], Jutta Winsemann [a]

[a] Institut für Geologie, Leibniz Universität Hannover, Callinstraße 30, 30167, Hannover, Germany
[b] Department of Geography and Geology, Geography Division, University of Turku, 20014, Turku, Finland
[c] Department of Remote Sensing and Photogrammetry, Finnish Geospatial Research Institute, National Land Survey of Finland, FI-02430, Masala, Finland
[d] Leichtweiß-Institut für Wasserbau, TU Braunschweig, Beethovenstraße 51a, 38106, Braunschweig, Germany

ARTICLE INFO

Article history:
Received 1 October 2018
Received in revised form
1 February 2019
Accepted 17 February 2019
Available online 1 March 2019

Keywords:
Glacial lake-outburst flood
Numerical flood simulation
Palaeotopography
Middle pleistocene glaciations
Ice-dammed lakes
Meltwater-drainage systems

ABSTRACT

The terrestrial margins of the Middle Pleistocene ice sheets in northern central Europe were characterised by the formation of extensive ice-dammed lakes, which were controlled by the blockage of spillways by the ice margin. The largest ice-dammed lake had a volume of ~224 km^3 and formed in a late stage of the first Saalian ice advance (MIS 6) in central Germany. The failure of the ice dam in the bedrock-outlet channel triggered a major glacial lake-outburst flood. Flood-related erosional and depositional features include large-scale scours, trench-like channels, streamlined hills, giant bars and run-up deposits, indicating a wide spreading of the outburst flood in an early stage and the incision of trench-like valleys in a later stage. The incision of large valleys in the proximal flood pathway strongly impacted the regional drainage system by providing an efficient drainage network. The trench-like channels initiated by the lake-outburst flood became a crucial part of the ice-marginal drainage and subsequent fluvial system.

The reconstructed outlet hydrographs imply peak discharges of 465,000–673,000 m^3s^{-1}. The numerical simulation indicates flow depths of up to 87 m, flow velocities of up to 7 ms^{-1}, peaks of the bed-shear stress of 2500 Nm^{-2} and the inundation of large parts of northwestern Germany and the northern Netherlands. The numerical simulation of the outburst flood was conducted on both the modern digital elevation model and on palaeotopographic models, representing the palaeotopography prior to the outburst flood and during maximum flood-related incision, respectively.

Distally, the outburst flood probably followed an east-west trending route through northwestern Germany and the central Netherlands into the ice-dammed lake in the southern North Sea Basin. The added water volume might have led to the overspill and drainage of the proglacial lakes in the central Netherlands and the North Sea Lake in a chain reaction, eventually opening an east-west trending meltwater-drainage pathway along the southwestern margin of the decaying ice sheet.

1. Introduction

Glacial lake-outburst floods are important geomorphologic drivers in modern and ancient glaciated systems. Flood-related erosion can have major impacts on the evolution of the large-scale drainage system due to the incision of deep channels and the breaching of drainage divides (Mangerud et al., 2004; Gupta et al., 2007, 2017; Collier et al., 2015; Komatsu et al., 2016). The largest glacial lake-outburst floods that have been extensively studied occurred in North America (e.g., Baker, 1973, 2009; Kehew and Lord, 1986; Teller et al., 2002; Alho et al., 2010; Curry et al., 2014) and Siberia (e.g., Carling et al., 2002; Herget, 2005; Margold et al., 2018). Smaller-scale glacial lake-outburst floods or jökulhlaups are for example known from Iceland (Russell and Knudsen, 1999; Marren and Schuh, 2009; Alho et al., 2005) and glaciated mountainous regions (Perkins and Brennand, 2014; Rosenwinkel et al., 2017). All these well-documented examples occurred during the Late Pleistocene or Holocene, commonly

* Corresponding author.
E-mail address: lang@geowi.uni-hannover.de (J. Lang).

https://doi.org/10.1016/j.quascirev.2019.02.018

allowing for the preservation of a substantial geomorphologic record. In contrast, fewer examples exist for large-scale glacial lake-outburst floods related to older glaciations, where the geomorphologic record has commonly been removed by subsequent erosion. Studies of these older outburst-flood events have to rely on deep erosional structures and flood-related deposits, which are commonly buried and/or patchily preserved (Froese et al., 2003; Gupta et al., 2007, 2017; Meinsen et al., 2011; Lang and Winsemann, 2013; Collier et al., 2015; Winsemann et al., 2016).

A powerful tool for palaeo-flood research is the numerical simulation of the floods. The results of these models allow for the quantification of the flood dynamics and the identification of the most likely flood pathway. Numerical flood simulations should be integrated with the geomorphologic and sedimentary evidence of outburst floods, which may provide constraints for water levels, flow depths, flow regimes and the ability to erode or deposit sediment. Vice versa, the output of numerical flood simulations provides indicators for potential zones of erosion or deposition, which may be overlooked in field or remotely sensed data. Approaches to the numerical simulation of glacial lake-outburst floods include (i) calculations of discharges and hydrographs in outlet channels (Carling et al., 2010; Herget et al., 2015; Margold et al., 2018), (ii) models of the flow dynamics within draining reservoirs (Alho et al., 2010; Bohorquez et al., 2016), and (iii) reconstructions of inundation and flow dynamics within the flood pathway (Alho et al., 2005; Denlinger & O'Connell, 2010; Winsemann et al., 2016). Calculations of discharges and hydrographs commonly comprise 1D models, while reservoir drainage and flood pathways generally require 2D models. In this study, a combined approach is applied to the simulation of a glacial lake-outburst flood, which integrates hydrographs derived from 1D numerical modelling of the dam breach with the 2D numerical simulation of the flood pathways. This combined approach allows for realistic boundary conditions and the simulation of the potential spatial and temporal flow pattern (e.g., Winsemann et al., 2016).

The aim of this study is to improve the understanding of glacial lake-outburst floods and their impacts along the Middle Pleistocene Saalian ice margin in northern central Europe. Although the formation of large ice-dammed lakes in the study area has long been known (e.g., Eissmann, 1975, 2002; Gassert, 1975; Thome, 1983; Herget, 1998, 2002; Junge, 1998; Winsemann et al., 2007, 2009, 2011a, b, 2018; Meinsen et al., 2011; Lang et al., 2018), the drainage of these lakes and their impact on the syn-glacial and post-glacial drainage network has yet received little attention (Meinsen et al., 2011; Winsemann et al., 2016). The study area holds a key position between the lowlands of northwestern Germany and the Netherlands, which extended into the North Sea Basin during the Pleistocene sea-level lowstands, and the more mountainous regions of eastern Germany, the Czech Republic and Poland. Ice-damming in the study area probably impacted the meltwater-drainage pathways up to the drainage divide between the Atlantic and the Black Sea in eastern Poland. Building on previous studies by Winsemann et al. (2007, 2009, 2011a, b), Meinsen et al. (2011) and Lang et al. (2018), who reconstructed the characteristics and evolution of ice-dammed lakes along the southwestern margin of the Middle Pleistocene (Saalian) Fennoscandian ice sheets, this study aims to (i) summarise the field evidence for a major glacial lake-outburst flood during the retreat of the first Saalian ice margin, (ii) estimate flood inundation and flow characteristics from numerical flood simulation, and (iii) discuss the impact of flood-related features on the meltwater-drainage pathways and river courses.

2. Regional setting

The study area is located in northern central Europe at the former southwestern margin of the Middle Pleistocene Fennoscandian ice sheets (Fig. 1A). The area is characterised by the transition from the relatively steep river valleys and bedrock ridges of the Central German Uplands into the low-relief area of the North German Lowlands. Typically, ridges trend WNW to ESE and comprise Mesozoic or Palaeozoic bedrock. The structural trend of the bedrock ridges is generally related to deformation during a phase of basin inversion in the Late Cretaceous (Betz et al., 1987; Lohr et al., 2007; Brandes et al., 2013). The Mesozoic bedrock ridges mostly represent salt-cored anticlines related to rising Permian salt (Kockel, 1991; Brandes et al., 2012, 2013).

During the Middle Pleistocene the study area was affected by multiple ice advances of the Elsterian and Saalian glaciations (Fig. 1A and B). Two major ice advances are known for the Elsterian glaciation, which advanced to approximately the same maximum position (Caspers et al., 1995; Junge, 1998; Eissmann, 2002; Litt et al., 2007; Ehlers et al., 2011; Lang et al., 2012; Roskosch et al., 2015). Three major ice advances are known from the older Saalian glaciation, which reached similar maximum extents but were characterised by different ice-advance directions and source areas (Eissmann, 1975, 2002; Ehlers, 1990; Skupin et al., 1993; Lang et al., 2018). Numerical ages of glacigenic and glacial lake-outburst flood deposits range from 196 ± 19 to 139 ± 8 ka (Busschers et al., 2008; Roskosch et al., 2015; Winsemann et al., 2015, 2016; Lang et al., 2018; Lauer and Weiss, 2018) and thus indicate that all these Saalian ice advances occurred during MIS 6 (Fig. 1B). However, some numerical ages exist that suggest an earlier Saalian ice advance during MIS 8 or early MIS 6 (Beets et al., 2005; Hall and Migoń, 2010; Kars et al., 2012; Roskosch et al., 2015). The third older Saalian ice advance represents a phase of re-advance and ice streaming, probably related to the drainage of ice-dammed lakes (Meinsen et al., 2011; Winsemann et al., 2011b). The subsequent ice advances of the middle and younger Saalian glaciations (Warthe) terminated northeast of the study area (Fig. 1A) (Ehlers et al., 2011). Numerical ages of glacigenic deposits of these ice advances range from 155 ± 21 to 130 ± 17 ka, thus also correlating with MIS 6 (Fig. 1B) (Lüthgens et al., 2010; Kenzler et al., 2017).

Saalian glacigenic deposits in the study area include subglacial tills, coarse-grained meltwater deposits and fine-grained lake-bottom sediments. Widespread glacilacustrine deposits bear evidence for the formation of ice-dammed lakes along the ice margin (Eissmann, 1975, 2002; Thome, 1983; Klostermann, 1992; Junge, 1998; Junge et al., 1999; Reinecke, 2006; Winsemann et al., 2007, 2009, 2011a, b, 2016; Lang et al., 2018). Extensive ice dammed lakes include the Münsterland, Weser and Leine Lakes in the west (Winsemann et al., 2007, 2009, 2011a, b, 2016; Meinsen et al., 2011), the Subhercynian Lake in the centre (Reinecke, 2006; Lang et al., 2018) and the Halle-Leipzig Lake (Lang et al., 2018) in the east of the study area (Fig. 2). The extents and volumes of the ice-dammed lakes and their evolution during the different older Saalian ice advances were reconstructed by Lang et al. (2018).

The largest ice-dammed lake in study area formed in the eastern part of the study area ("Halle-Leipzig Lake"). During the maximum extent of the first Saalian ice advance lake levels of up to 350 m a.s.l. were attained in isolated lakes in the river valleys south of the ice margin, including the Saale-Unstrut Lake (Fig. 2A) (Lang et al., 2018). Successive ice-margin retreat allowed for the connection of these lakes to form the more extensive Halle-Leipzig Lake (Fig. 2C and D). The maximum lake volume of ~224 km^3 was attained during a later stage of ice-margin retreat (Fig. 2D). The formation of the Halle-Leipzig Lake was controlled by a WNW-ESE trending ridge of Palaeozoic and Mesozoic bedrock ("Rothenburg anticline"), which has an elevation of 140–230 m a.s.l. (Fig. 3A). When an advancing ice sheet reached this bedrock ridge all northwards directed drainage pathways were blocked (Lang et al., 2018).

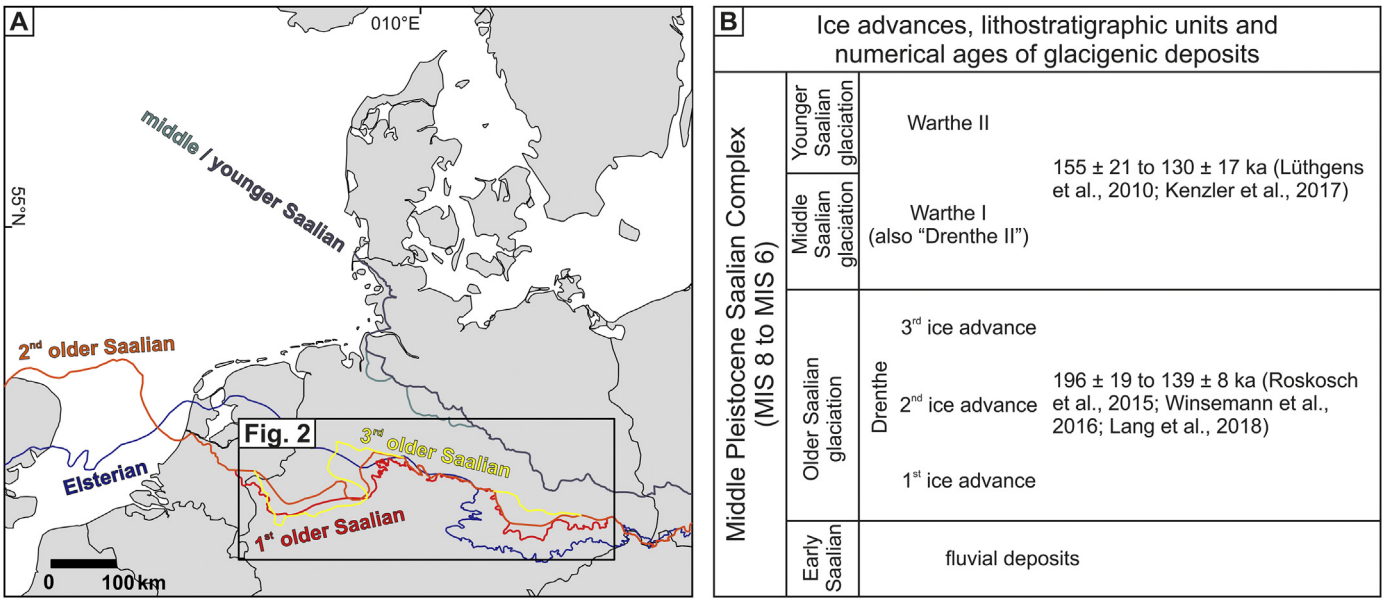

Fig. 1. A) Overview map, showing the maximum extent of the Middle Pleistocene ice advances into northern central Europe. Ice margins are compiled from Ehlers et al. (2011), Winsemann et al. (2011b), Moreau et al. (2012) and Lang et al. (2018). **B)** Stratigraphic chart for the Middle Pleistocene Saalian complex.

Overspill channels had elevations of 150–178 m a.s.l. and controlled the lake level. Today, the bedrock ridge is dissected by the V-shaped gorge of the River Saale, which is incised by as much as 100 m to ~60 m a.s.l. (Fig. 3A). Reconstructions of the evolution of the regional drainage network suggest that this gorge developed during the Middle Pleistocene glaciations. All pre-glacial river courses ran east of the bedrock ridge, while the courses of the River Saale and its tributaries were redirected through the gorge during the glaciations (Schulz, 1962; Knoth, 1964; Ruske, 1963, 1973; Wansa, 1997). The gorge was probably initiated by overspills or outburst floods from the Elsterian ice-dammed lakes. The opening of the ice dam in the River Saale gorge led to the complete drainage of the lake.

Lake formation recurred during the second Saalian ice advance, which had a lesser maximum extent. Glacifluvial deltas indicate a lake level of ~160 m a.s.l. during the maximum ice extent. These delta deposits yielded luminescence ages of 175 ± 10 and 173 ± 19 ka (Lang et al., 2018). The retreat of the ice margin probably led again to an increase in lake area. It is not clear if the ice-dammed lake drained at this stage or if it persisted until the third Saalian ice advance (Lang et al., 2018). The third Saalian ice advance into the Halle-Leipzig area probably represented a minor re-advance (Eissmann, 1975, 2002).

3. Methods

3.1. Mapping of flood-related features

Flood-related erosional and depositional features were mapped from high-resolution digital elevation models (grid: 10 m, vertical accuracy: ± 1 m ("LGLN DGM-10") and grid: ~30 m, vertical accuracy: ~3 m ("EU-DEM")), geological maps (1:25,000, 1:50,000, 1:100,000) and borehole logs. All available data sets were integrated in a geographical information system (Esri ArcGIS, Version 10.3).

3.2. Reconstruction of the palaeotopography

The use of present day topographic models can be a major source of uncertainty in palaeoflood simulation (Miyamoto et al., 2006; 2007). Therefore, the palaeotopography for those parts of the inferred proximal flood pathway, where evidence of a strong geomorphic impact of the outburst flood is observed, was reconstructed. To construct palaeotopographic models the present day DEM (grid ~30 m, vertical accuracy ~3 m, EU-DEM) was modified, using information on the palaeotopography derived from geological maps and borehole data. The modification of the DEM was conducted in a 3D geological modelling software (SKUA-GOCAD), which allows the modification of selected regions of the DEM by using the available data as constraints. Two different palaeotopographic models were reconstructed, representing (i) the topography prior to major erosion by a glacial lake-outburst flood, and (ii) the topography at the phase of maximum incision during or immediately after the glacial lake-outburst flood.

The reconstruction of the palaeotopography benefits from the long research history of the study area and the availability of detailed maps, including the surface geology and the near surface Pleistocene deposits. The surface geology is based on the geological map by Look (1984). The base of the Pleistocene and the lithostratigraphic units are based on subsurface maps by Marcinkowski et al. (1973, 1982), Marcinkowski and Cepek (1982), Rosenberger et al. (1973) and Hinze et al. (1995). Borehole markers and contour lines from depth maps are used as main input data for the model. The modern day topography is used without modification, if the surface comprises bedrock or a thin layer of loess. Patchy occurrences of Pleistocene deposits and Holocene deposits at the bases of minor valleys are ignored.

3.3. Numerical flood simulation

The numerical simulation of the glacial lake-outburst flood was conducted in two steps, combining a 1D hydraulic model (HEC-RAS) of the flood hydrographs with a 2D hydraulic model (TUFLOW) of the flood inundation. This powerful approach for the simulation of palaeo-floods combines realistic boundary conditions with the potential spatial flow pattern (e.g., Winsemann et al., 2016).

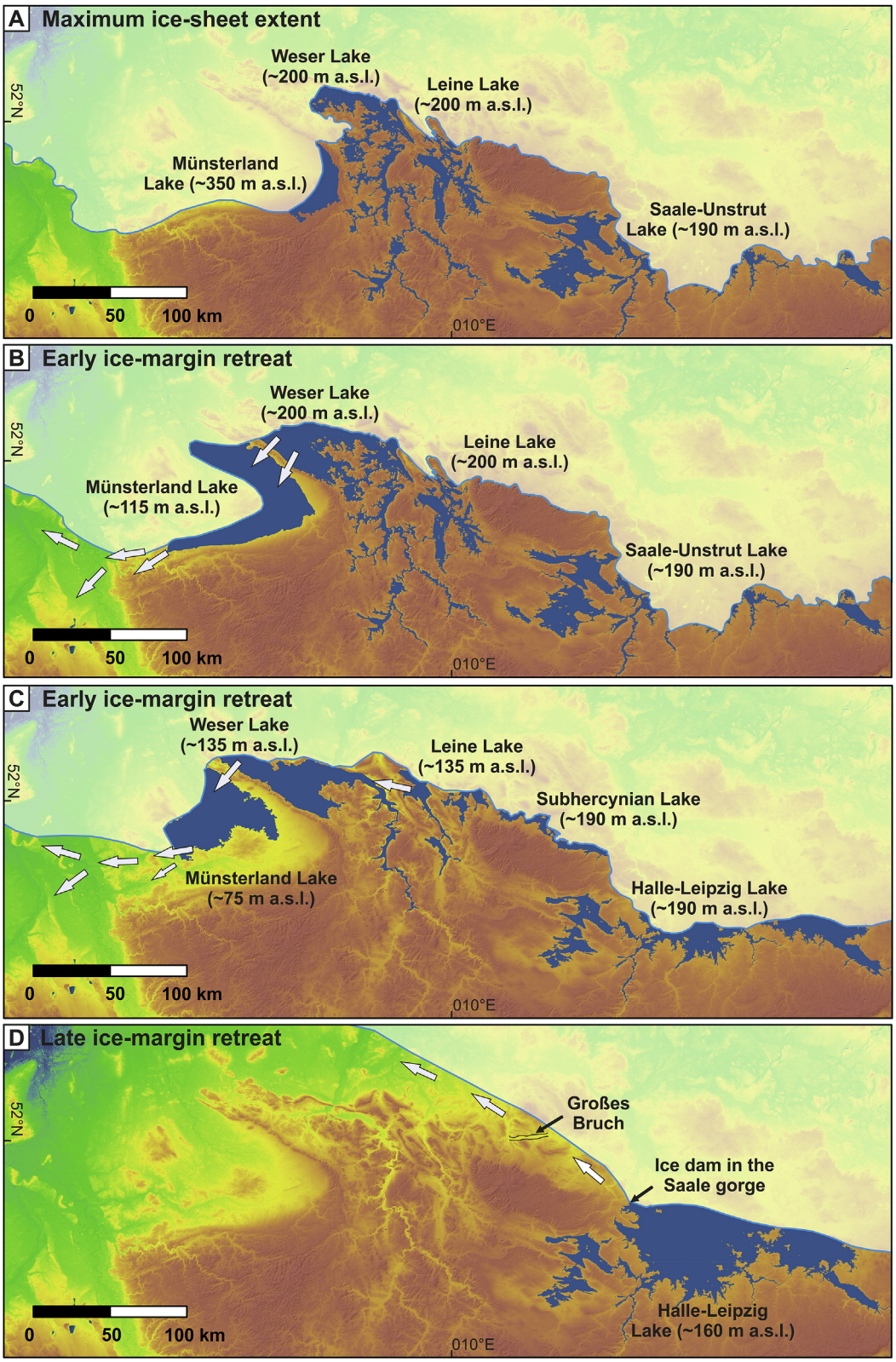

Fig. 2. Palaeogeographic reconstruction of ice-dammed lakes during the first older Saalian ice advance (modified from Winsemann et al., 2016; Lang et al., 2018). Arrows indicate glacial lake-outburst floods. **A)** Maximum ice-sheet extent. **B, C)** Early stage of ice-margin retreat. Lake-outburst floods occur from the Weser Lake into the Münsterland Lake, which subsequently drains towards the west. **D)** Late stage of ice-margin retreat. While the lakes in the west have already drained, a large lake (Halle-Leipzig Lake) has formed in the east and is controlled by an ice dam in the Saale gorge.

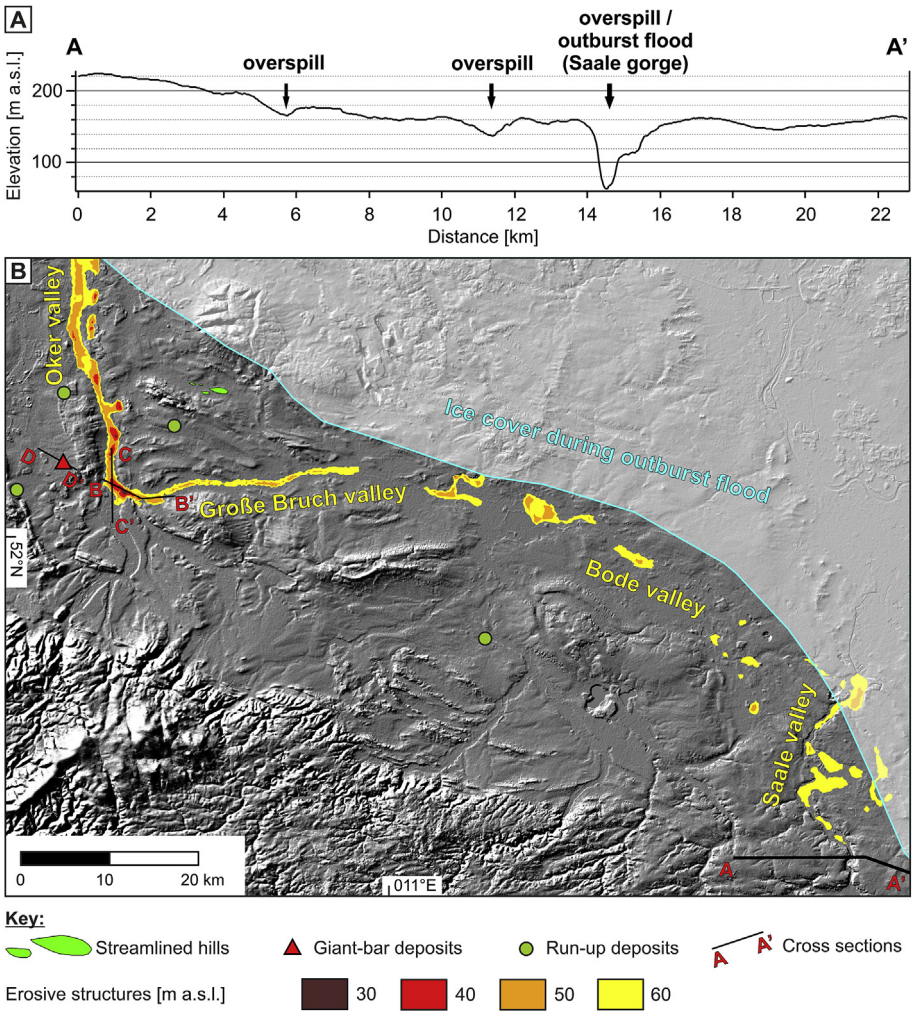

Fig. 3. A) Topographic cross section (AA′ in Fig. 3B) of the river gorge in the Saale valley. **B)** Distribution of erosional and depositional landforms in the proximal part of the flood pathway (cross sections BB′, CC′ and DD′ are shown in Fig. 4).

3.3.1. Calculation of the flood hydrographs (HEC-RAS)

The outlet hydrographs for the drainage of the Halle-Leipzig Lake were derived from a 1D hydraulic model (HEC-RAS), including an approximation of the dam-break process and the one-dimensional flood routing. The software solves the unsteady St-Venant equation in 1D or 2D (Brunner, 2016). In this research it was used in 1D-mode to approximate the outflow hydrograph for later use in the flood routing. The Halle-Leipzig Lake (Fig. 2D) was discretised one-dimensionally by extracting cross-sections of the modern digital elevation model. Inside the lake a main river course and three smaller tributaries were defined and coupled to a river network. The ice dam was modelled in HEC-RAS inside the Saale gorge by defining a dam (inline broad-crest weir, weir coefficient 1.4) in analogy to the work described in Winsemann et al. (2016). The dam had a crest level of 170 m a.s.l with a V-shaped breach geometry. The lowest breach level was defined by the modern topography inside the gorge (65 m a.s.l.). Since breach progression is hard to estimate, four durations (10 h, 25 h, 50 h, 100 h) were set after which the breach had completed. Downstream of the ice dam and inside the Saale valley the model domain was extended to stabilise the numerical solution. A pilot flow (constant initial discharge) seeping out of the ice dam was set to 1000 m^3/s to ensure that the cross sections downstream of the ice dam would not fall dry at any time during the simulation. The model extension downstream of the ice dam was constrained by the ice shield in the northeast and by the modern topography towards the southeast. Energy loss along the flow path is described in the St-Venant equation by Manning's coefficient n which was estimated as $n = 0.02$.

Winsemann et al. (2016) tested two different breach geometries and their effect on outflow hydrographs in a study focussing on outburst floods of the Weser and Münsterland Lakes (Fig. 2A and B). These authors found that breach geometries had little influence on the peak discharges and overall lake level dynamics. The major parameter to control the shape of the hydrographs was related to the dam-breach duration. The four durations tested in this study result in peak discharges ranging between 465,000 and 673,000 m^3s^{-1}. The outflow hydrographs were then used as input for 2D hydraulic simulations.

3.3.2. Simulation of flow routing and dynamics (TUFLOW)

The outburst flood from the Halle-Leipzig Lake was reconstructed with a 2D hydraulic simulation (TUFLOW Version 2018.03). TUFLOW simulates flow over a regular grid of square elements and is based on solving the fully 2D depth-averaged, momentum and continuity equations for free-surface flow using a 2nd order implicit matrix solver (Stelling, 1984; Syme, 1991; TUFLOW, 2017).

The grid used in the TUFLOW simulation had a cell size of 500 × 500 m. The elevation data for the grid are based either on the modern DEM (grid: ~30 m, vertical accuracy: ~3 m) or the reconstructed palaeotopographies, represented by manipulated DEMs. The calculated outflow hydrographs were used as upstream boundary conditions. Applying different hydrographs allows for testing the impact of the duration of the ice-dam failure and the resulting peak discharge on the routing and dynamics of the outburst flood. The downstream boundary condition is set to a constant water level of zero at the modern coast line, which represents the limit of the available topographic data. A further constraint is provided by the reconstructed ice margin, which is in large parts highly uncertain. Therefore, three different ice-margin configurations were tested. All grid cells in areas, which were ice covered during the outburst flood, are defined as inactive and can therefore not be flooded. Cells in upland areas at the southern margin of the model area were also defined as inactive to save computing time and memory.

TUFLOW calculates the eddy viscosity with the Smagorinsky formula, using default values of 0.5 for the dimensionless Smagorinsky coefficient and 0.05 m^2s^{-1} for the constant viscosity coefficient. The application of the Smagorinsky formula means that the viscosity coefficient is recalculated every timestep and will thus vary in space and time (TUFLOW, 2017). For all model runs, the computing timestep was set to 10s and the number of iterations to 2.

4. Results

4.1. Flood-related erosional and depositional features

Flood-related erosional and depositional features are prominent in the proximal flood pathway in the valleys of the Rivers Saale and Bode, the Groβe Bruch valley and the valley of the River Oker (Fig. 3B). A detailed description and interpretation of flood-related features is provided in Table 1. Erosional features include large-scale scours, trench-like valleys and streamlined hills. The deeply incised scours and trench-like valleys are commonly partly or completely buried by flood-related or post-flood deposits (Fig. 4A and B). Some scours seem to follow pre-existing structures or are associated with easily erodible substrates (Figs. 3B and 4A, B). However, the west-east-trending trench-like valley of the Groβe Bruch cross-cuts pre-existing bedrock ridges related to salt-cored anticlines (Fig. 3B). Flood-related deposits include a giant bar associated with slackwater deposits and run-up deposits (Figs. 3B and 4C, Table 1). These deposits occur in flooded tributary valleys and slopes exposed towards the flow direction, respectively. The compositions of the giant-bar and run-up deposits points to reworking and mixing of older fluvial and glacigenic deposits.

4.2. Palaeotopographic models

The palaeotopographic models focus on the areas of the Bode valley, the Groβe Bruch valley and the Oker valley (Fig. 5), which represent the main flood pathway and have the thickest Pleistocene deposits in the study area.

4.2.1. Palaeotopography prior to flood-related incision ("pre-incision model")

The first palaeotopographic model was reconstructed to represent the topography along the assumed flood pathway prior to major flood-related incision (Fig. 5B, D). The reconstruction of this palaeotopographic model is based on the assumption that flood-related incision dissected a flat-topped fluvial terrace comprising pre-flood (i.e., early Saalian) braided river deposits. Remnants of this fluvial terrace occur at the margins of the Bode, Groβe Bruch and Oker valleys (cf., Look, 1984). The elevations of these fluvial terraces were used to interpolate the pre-flood elevations of the valleys. In areas, where the top of the early Saalian fluvial terrace is covered by younger deposits, the elevation is provided by borehole markers. The reconstructed pre-incision palaeotopography is characterised by a more gentle topography and less pronounced valleys (Fig. 5B). Large parts of the Bode, Groβe Bruch and Oker valleys are infilled by fluvial deposits. The drainage divide between west and east in the Groβe Bruch valley, which is very subtle today, is more pronounced.

4.2.2. Palaeotopography during the maximum flood-related incision ("maximum incision model")

The second palaeotopographic model was reconstructed to represent the topography along the assumed flood pathway during the stage of maximum incision (Fig. 5C, E). Borehole markers used to reconstruct the surface of maximum incision represent either the base of the Pleistocene or the eroded top of Pleistocene pre-flood deposits (i.e., Saalian till, early Saalian fluvial deposits or Elsterian deposits). For the largest part of the modelled area the palaeotopography represents the base of the Pleistocene succession. In the Saale valley the topography is characterised by elongate scours, which are incised into bedrock (Fig. 5C). In the Bode valley, the modelled palaeotopography corresponds to the top of the pre-flood deposits, which include Saalian till, early Saalian fluvial deposits and Elsterian deposits. In this area, the topography displays isolated scours. Towards the northwest, scours evolve into broad channel-like depressions (Fig. 5C). Farther to the west, in the Groβe Bruch and Oker valleys, the palaeotopographic surface again represents the base of the Pleistocene succession. In this area the palaeotopography is characterised by a continuous channel (Fig. 5C), displaying localised overdeepenings and topographic steps. The channel trends east-west in the Groβe Bruch valley and bends sharply into in the Oker valley and attains a south-north trend. At the junction of the Groβe Bruch and Oker valleys, a deep scour is developed. In the Oker valley, elongate scours occur east of the main channel course (Fig. 5C).

4.3. Results of the numerical flood simulation

A total of 22 flood simulations with different input parameters were conducted to test the impact of the different parameters, including (i) outlet hydrograph, (ii) surface roughness (Manning's n), (iii) the topography of the model area, and (iv) the ice-margin configuration. The results extracted from the 2D numerical simulation include the inundation pattern, water-level elevation (or flow depth, respectively), flow velocity, bed-shear stress and Froude number.

4.3.1. Impact of outlet hydrographs and surface roughness

Four different outlet hydrographs were applied as upstream boundary condition for the 2D numerical simulation to test their impact on the spreading of the flood and the flow dynamics. The peak discharges of the different outlet hydrographs range from 465,000 to 673,000 m^3s^{-1} with dam-breach durations between 10 and 100 h (Fig. 6), resulting in the complete drainage of the lake within six to nine days. The different applied outflow hydrographs impact the maximum flow velocity and the timing of the maximum water depth at different locations in the model area, while the impact of the hydrographs on the magnitude of the maximum water depth is very low. Higher peak discharges, which correspond to a faster dam breach, result in an earlier attainment of the peaks in water depth and flow velocity. The magnitudes of the water depth and the flow velocity increase at high peak discharges

Table 1
Flood-related erosional and depositional features.

Description	Interpretation
Erosional features	
Scours: Large-scale scours occur in the valleys of the rivers Saale, Bode and Oker and are incised into bedrock or unconsolidated Cenozoic or Pleistocene deposits. (Fig. 3B). In the Saale valley up to 15 m deep scours are observed, which mostly trend northwest-southeast and are 1.5–3.2 km long, 0.7–1.4 km wide and have mean aspect ratios (length/width) of 2.4. In the Bode valley, isolated, 5–25 m deep scours occur, which are 0.5–2 km long, 0.5–1.1 km and have mean aspect ratios (length/width) of 1.3. The largest individual scour occurs at the confluence of the Groβe Bruch and Oker valleys. This scour is up to 30 m deep and curves northwards into the Oker valley (Figs. 3B and 4A, B).	Scours point to intense erosion in zones of flow expansion or confluence, where strong turbulent eddies develop (Best and Roy, 1991; Hoyal et al., 2003; Carling et al., 2009a, b; Winsemann et al., 2016). In fluvial systems such scours can reach four to five times the average channel depth (Best and Ashworth, 1997; Ullah et al., 2015). Channel-like scours indicate longer-term erosion in preferential flow pathways. Scouring typically is focused in areas of easily erodible substrates.
Elongate channel-like scours occur in the Bode valley. They trend WNW-ESE, are 4.3–6.8 km long, 0.8–2 km wide and are 20–30 m deep. The channel-like scours display anastomosing pattern and are separated by higher, relatively flat areas.	
Trench-like valleys: The Groβe Bruch valley is a west-east trending trench-like valley, which is 40 km long 2–3 km wide and 20–60 m deep (Fig. 3B). The valley has a U-shaped geometry with very steep margins and is incised into Mesozoic bedrock, Palaeogene deposits and Pleistocene deposits. The dissection of early Saalian fluvial deposits and Saalian till indicates an incision during a late stage of the Saalian glaciation (Look, 1984; Feldmann et al., 2001; Weymann et al., 2005). The base of the valley is undulating with local overdeepened scours, which are up to 20 m deeper than the average valley base (Figs. 3B and 4A). The main valley fill comprises sand, pebbly sand and gravel, with intercalations of up to 10 m thick units of locally organic-rich mud (Fig. 4A). The basal valley fill is commonly fine-grained and comprises locally derived clasts, indicating short transport distances (Koch, 2015). The clast composition of the upper coarse-grained units is characteristic of meltwater deposits (Feldmann et al., 2001; Koch, 2015). The uppermost valley fill comprises 1–10 m thick, fine-grained organic-rich deposits of fens and small streams.	The Groβe Bruch and Oker valleys represent deeply incised flood spillways. The geometries and width-to-depth ratios match the straight, trench-like channels incised by glacial lake-outburst floods (Baker, 1973; Kehew and Lord, 1986; Carling et al., 2009a; Meinsen et al., 2011; Curry et al., 2014). The incision of straight, steep-walled channels relates to highly erosive flows with low sediment load and a resistant substratum (Kehew and Lord, 1986). Even coarse-grained sediment may be transported as suspended load in such high-energy flows (Carling, 2013), favouring the development of narrow, steep-walled channels (Kehew and Lord, 1986). The undulating basal profile of the channel with alternating deep scours and shallow sections is interpreted as relating to the lithology of the subcropping bedrock. More resistant lithologies formed lateral constrictions and elevated steps. Flow expansion downflow of such constrictions leads to intense turbulence and erosion, allowing for the formation of deep scours (Hoyal et al., 2003; Carling et al., 2009a, b; Winsemann et al., 2016). Alternations of narrow and wide channel sections are characteristic of channels related to high-magnitude floods (Baker, 2009; Carling et al., 2009a). Elevated steps related to resistant bedrock may form cataracts and retreating knickpoints, which foster the incision of a channel (Carling et al., 2009a).
To the west the Groβe Bruch valley joins the north-south trending Oker valley. Upstream of the confluence, the base of the Oker valley is characterised by a gently northwards-dipping, flat basal surface, displaying a V-shaped cross-sectional geometry, and a gravel-dominated infill. Downstream, the Oker valley is broader and more U-shaped and several overdeepened scours occur. The infill in this part of the valley is more heterogeneous, consisting of mud, sand, pebbly sand and gravel (Fig. 4B).	
Streamlined hills: North of the Groβe Bruch valley several streamlined hills occur (Fig. 3B). The streamlined hills are lemniscate with the more blunted end towards the ESE and the more pointed end towards the WNW. Some of them display a shallow moat at the blunt end. The hills are 0.4–2.2 km long, 0.15–0.6 km wide and have aspect ratios (length vs. width) between 2.6 and 3.7. The height of the hills is between 2 and 13 m with very smooth topographies. The largest hill comprises Lower Cretaceous marlstone, while the smaller hills comprise Pleistocene sandy and gravelly meltwater deposits (Look, 1984).	The lemniscate geometry, smooth topography and aspect ratios of the streamlined hills is interpreted as pointing to the formation under high-discharge, fully submerged conditions (Patton and Baker, 1978; Komar, 1983; Meinsen et al., 2011; Collier et al., 2015). Their orientation with the blunt end pointing ESE is consistent with the flow direction of the lake-outburst flood. The shallow moat at the blunt end indicates scouring in front of an obstacle (Carling et al., 2009a).
Depositional features	
Giant bar: The thickest flood-related deposits occur in the lee of a bedrock ridge east of the Oker valley, which is located opposite to the confluence of the Groβe Bruch and the Oker valley. At the southern end of this bedrock ridge a large-scale bar is observed that has a maximum elevation of 151 m a.s.l. and is ~5 km long (Figs. 3B and 4C). The distal side of the bar is very smooth and dips to the northwest. Borehole data indicate very heterogeneous deposits, including diamicton, gravel, pebbly sand, sand and mud, and a lateral fining of the deposits towards the northwest (Fig. 4C). Previous studies noted an unusual composition, comprising a very large proportion of clasts characteristic for the regional fluvial deposits in combination with up to boulder-sized erratic clasts (Dahlgrün, 1939). The up to 45 m thick succession overlies early Saalian fluvial deposits. In several boreholes north of the bar, 1–4 m thick beds of mud are present, which directly overlie the bedrock.	The thick deposits opposite of the confluence of the Groβe Bruch and the Oker valley are interpreted as a giant bar, representing a characteristic feature of outburst floods spreading through confined valleys (Carling et al., 2002, 2009b; Herget, 2005; Carling, 2013). The formation of giant bars is related to flow expansion and eddy formation in backflooded tributary valleys (Herget, 2005). Both bedload and suspended load are deposited by underflows at the lee side of the giant bar, forming large-scale clinoforms dipping into the tributary valley (Carling et al., 2002, 2009b; Carling, 2013). The complex internal structure of the giant bars, which includes a broad spectre of grain sizes, is related to flow pulsations (Carling et al., 2002). Fine-grained deposits on the distal side of the bar probably represent slack-water deposits due to ponding (Herget, 2005). The unusual clast composition of the giant bar points to reworking and mixing of older fluvial and glacigenic deposits (Winsemann et al., 2016).
Run-up deposits: Patchy occurrences of flood-related deposits were mapped at several locations (Fig. 3B) on the flanks of bedrock ridges, occurring at elevations between 144 and 157 m a.s.l. These deposits typically form less than 1 m thick sheets that comprise interbedded sand and gravel. Previous studies noted unusual clast compositions, which are characterised by a mixture locally derived and erratic clasts (Woldstedt, 1931; Rosenberger et al., 1973).	Patchy occurrences of sand and gravel are interpreted as run-up deposits that are typically deposited at slopes exposed towards the flow direction and represent the highest level of flood deposition (Herget, 2005; Carling et al., 2010). The unusual clast composition of the run-up deposits points to reworking and mixing of older fluvial and glacigenic deposits (Winsemann et al., 2016).

(Figs. 7A and 8).

All further described simulation results for flood spreading and flow dynamics are based on the hydrograph characterised by a dam-breaching duration of 50 h and a peak outlet discharge of 502,000 m^3s^{-1}.

Three different values for the bed roughness (Manning's n) were tested in the flood simulation (n = 0.03, 0.07 and 0.1; Fig. 7B). Increasing the bed roughness lowers the flow velocity, leading to an increase in water-level elevation (or flow depth, respectively) and a delayed passage of the flood peak at an observation point due to the increased flow resistance (cf., Carrivick, 2010). The results of the 2D numerical simulation indicate that the bed roughness has a larger impact on the maximum water levels and flow velocities than the different hydrographs (Fig. 7A and B).

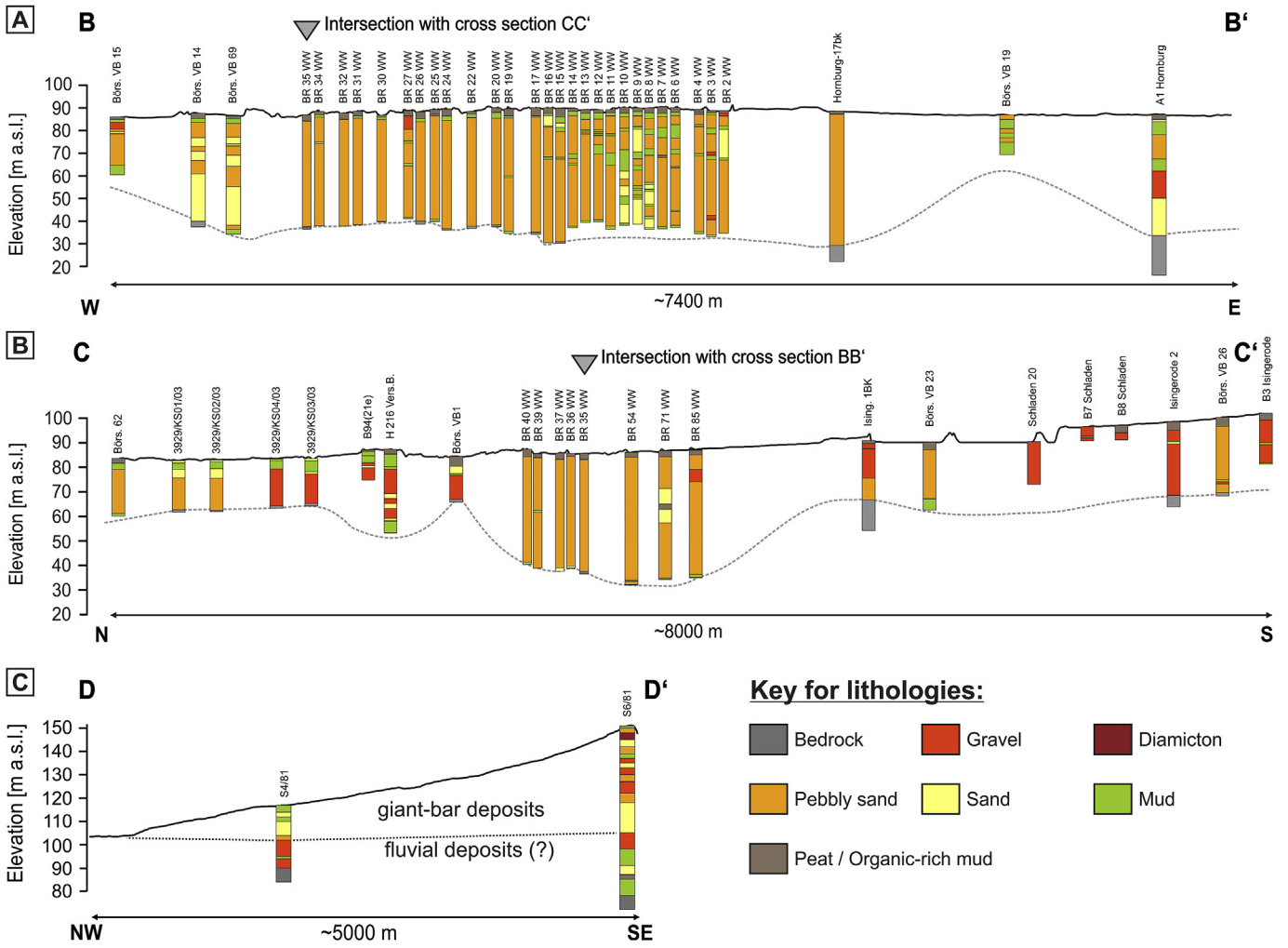

Fig. 4. Geologic cross-sections based on borehole data. The locations of the cross sections are provided in Fig. 3B. **A)** Cross-section (BB′) of the Groβe Bruch valley. The base of the Pleistocene is extracted from the 3D subsurface model. **B)** Cross-section (CC′) of the Oker valley. The base of the Pleistocene is extracted from the 3D subsurface model. **C)** Cross-section (DD′) of a giant bar west of the confluence of the Groβe Bruch and the Oker valleys.

A value of 0.07 for Manning's n provides the best fit for the geomorphic evidence. All further described simulation results on flood spreading and flow dynamics are based on a bed roughness with a value of 0.07 for Manning's n.

4.3.2. *Inundation pattern*

The main constraint for the flood pathway is the margin of the retreating ice sheet. In general, the outburst flood follows the ice margin towards the northwest (Figs. 9 and 10), because the overall topography of the study area is gently sloping towards the north or northwest. In the proximal flood pathway it follows the Bode valley and adjacent, northwest-southeast trending structural valleys. The Groβe Bruch valley directs a large part of the flood towards the west. The various branches of the flood rejoin when entering the north-south trending Oker valley. Westwards of the Oker valley, the topographic confinement of the flood is reduced and the spreading flood inundates a 45–60 km wide area between the ice margin and the northern margin of the Central German Uplands. The outburst flood follows the pathways predefined by the (modern) topography, which was of course subject to post-flood modification, and the ice margin. In all three tested ice-margin configurations the main flood pathway is always next to the ice-margin. Several west-east to northwest-southeast trending topographic depressions in northwestern Germany and the Netherlands, which are located between Saalian till plateaus (Fig. 11D), act as main pathways for the simulated flood and are characterised by high flow depths and velocities.

The numerical flow simulation of the spreading of the outburst flood indicates maximum flow depths of up to 87 m, flow velocities of up to 7 ms^{-1} and peaks of the bed-shear stress of up to 2500 Nm^{-2}. The water depth in the inundated area is strongly controlled by the underlying topography (Figs. 7C, 10 and 11). The temporal evolution of the water depth was extracted at six locations that display very similar pattern. An initial very rapid rise of the water depth towards the peak is followed by a slow recession (Fig. 8). The highest water depths of 60–87 m occur in the most proximal flood pathway in the Saale and Bode valleys. This area is also characterised by low flow velocity (<2 ms^{-1}) and bed-shear stress (<100 Nm^{-2}) (Fig. 9B and C), which is probably related to a backwater effect when the flood transitions from the broad Bode valley into narrower valleys constrained by steep bedrock ridges. Zones of high flow velocity (5-7 ms^{-1}) and bed-shear stress (1000–1500 Nm^{-2}) occur in areas where the flow is laterally or vertically confined by the local topography (Fig. 9B and C). Broad zones of high bed-shear stress across the main flow direction commonly correspond to the drainage divides that are crossed by the outburst flood. The strongest channelisation of the flood occurs when it follows the course of the Groβe Bruch and Oker valleys (Fig. 10A, C). Flow

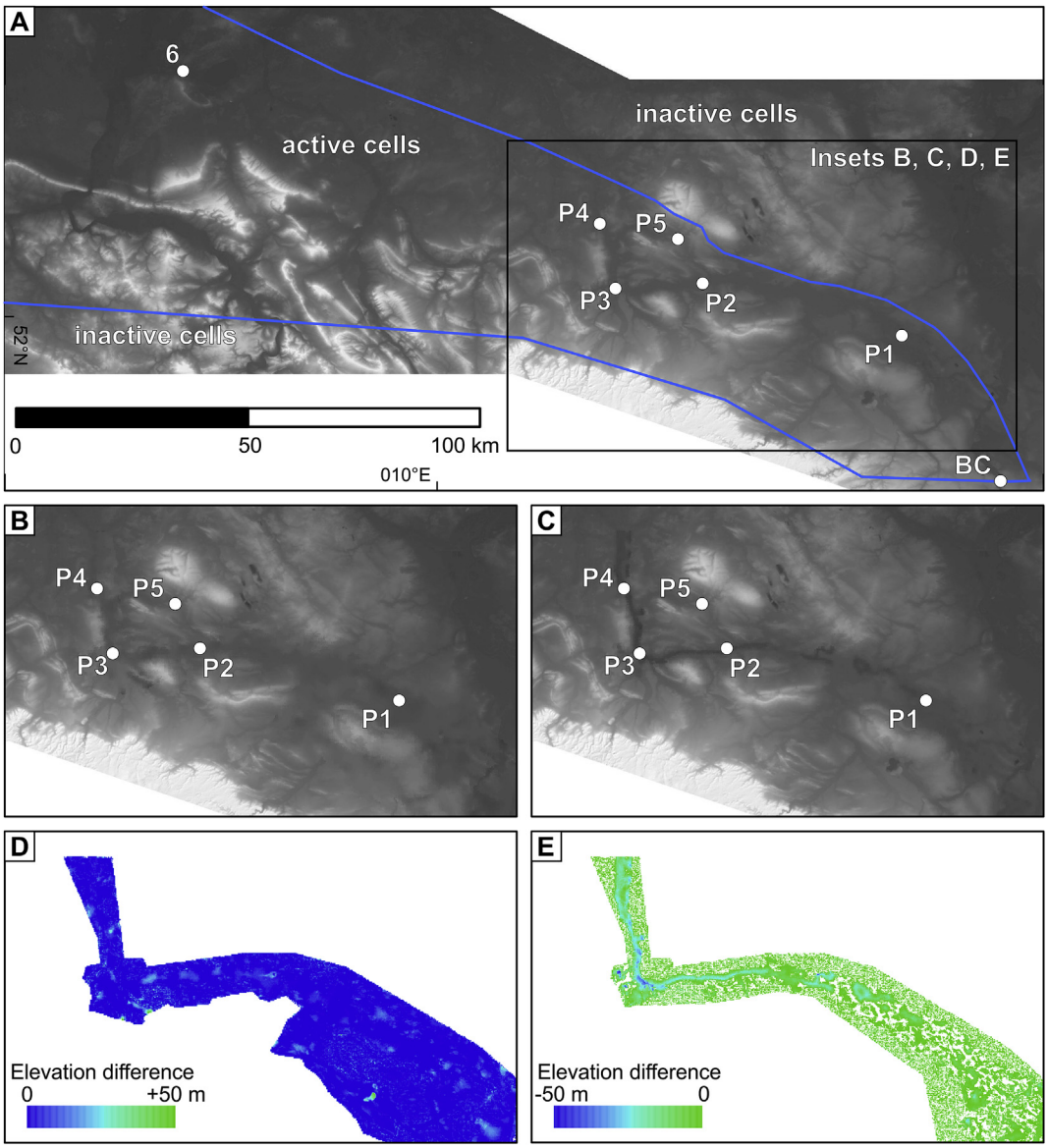

Fig. 5. A) Set-up of the 2D flood simulation on the modern digital elevation model. The blue line shows the extent of the model area (active cells). "BC" marks the location of the Saale gorge, where the flood hydrographs are applied as upstream boundary conditions. "P1" to "P5" indicate the locations of the observation points, where the water level during the simulation is extracted (P1: Bode valley; P2: Groβes Bruch valley; P3: confluence of the Groβe Bruch and Oker valleys; P4: northern widening of the Oker valley; P5: location of streamlined hills; P6: distal flood pathway). **B)** Reconstruction of the palaeotopography prior to flood-related incision. Location is given in Fig. 5A. **C)** Reconstruction of the palaeotopography at the stage of maximum flood-related incision. Location is given in Fig. 5A.**D)** Difference in elevation between the modern topography and the reconstructed pre-incision palaeotopography. **E)** Difference in elevation between the modern topography and the reconstructed maximum incision palaeotopography. (For interpretation of the references to colour in this figure legend, the reader is referred to the Web version of this article.)

conditions are generally subcritical, because the large flow depths require very high velocities to attain supercritical flow conditions (Fig. 9D). Supercritical flow conditions occur at very few locations were the flow is constricted by the topography. One of these locations corresponds to the observed streamlined hills (Fig. 3A), where supercritical flows with Froude numbers larger than two were observed in all simulations.

The use of the reconstructed palaeotopographies in the simulations results in similar large-scale inundation patterns (Fig. 10). The pre-incision models display more and deeper inundation in the area between the Groβe Bruch valley and the ice margin and in the north-south trending valley west of the Oker valley (Fig. 10B). In contrast, the maximum incision models display a very strong channelisation of the flood through the Groβe Bruch and Oker valleys (Fig. 10C). These differences can also be observed when comparing the maximum flow velocities and bed-shear stresses (Fig. 10D and E). In the pre-incision models peaks of the flow velocity and the bed-shear stress occur at confinements to the spreading outburst flood. In contrast, in the maximum incision models the highest values for the flow velocity and the bed-shear stress are attained in the area of strong channelisation in the Groβe Bruch and Oker valleys.

5. Discussion

5.1. Numerical flood simulation

The major limitations for the numerical simulation of past outburst floods are (i) the limited information on the palaeotopography, and (ii) the failure to account for flood-related erosion

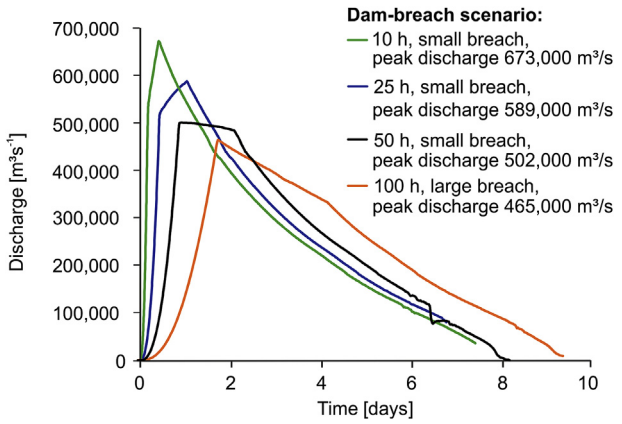

Fig. 6. Flood hydrographs derived from the model of the ice-dam failure (HEC-RAS) for four different breach-formation times (10, 25, 50 and 100 h) and two breach widths.

and deposition (Miyamoto et al., 2006, 2007; Alho et al., 2010; Winsemann et al., 2016; Margold et al., 2018). In the study area, this problem became more distinct due to the underfilled channel of the Groβe Bruch valley, which forms a pronounced topographic valley and thus receives a large part of the flood discharge in model runs based on the modern topography (Fig. 10A). To overcome this limitation, the pre-flood palaeotopography of the area most affected by flood-related geomorphologic features was reconstructed. The pre-flood palaeotopography allows for the simulation of flood inundation before major erosion occurred. Palaeotopographic models as a base for numerical flow simulation have previously been applied by Beeson et al. (2017), who used reconstructed bathymetries in the simulation of turbidity currents triggered by the Missoula flood off the west coast of North America. Other studies limited the reconstruction of topographies to the removal of artificial features (Denlinger & O'Connell, 2010). The available data on the surface and subsurface geology of the study area allowed for the construction of palaeotopographic models. Although the data base remains a limitation to the robustness of the palaeotopographic models, the data density is highest in the areas that were most affected by the outburst flood. Furthermore, in the hydraulic simulations the input grid is coarsened to a cell size of 500 × 500 m, which is much coarser than the cell size commonly used by topographic models.

The comparison of the simulations indicates that the tested parameters have a minor impact on the overall inundation pattern. Considerable differences between the results occur only if different basal topographies or ice-margin configurations are used (Figs. 9 and 10). Basal topography represents the main controlling factor for flood inundation (cf., Denlinger & O'Connell, 2010). The modern topography is considered to be an adequate base for palaeo-flood modelling, as has been shown in previous studies (e.g, Denlinger & O'Connell, 2010; Alho et al., 2010; Winsemann et al., 2016). However, even the use of a limited palaeotopographic model represents an improvement compared to the use of the modern topography as input for the hydraulic simulation, especially if large-scale flood-related features in the modern topography are

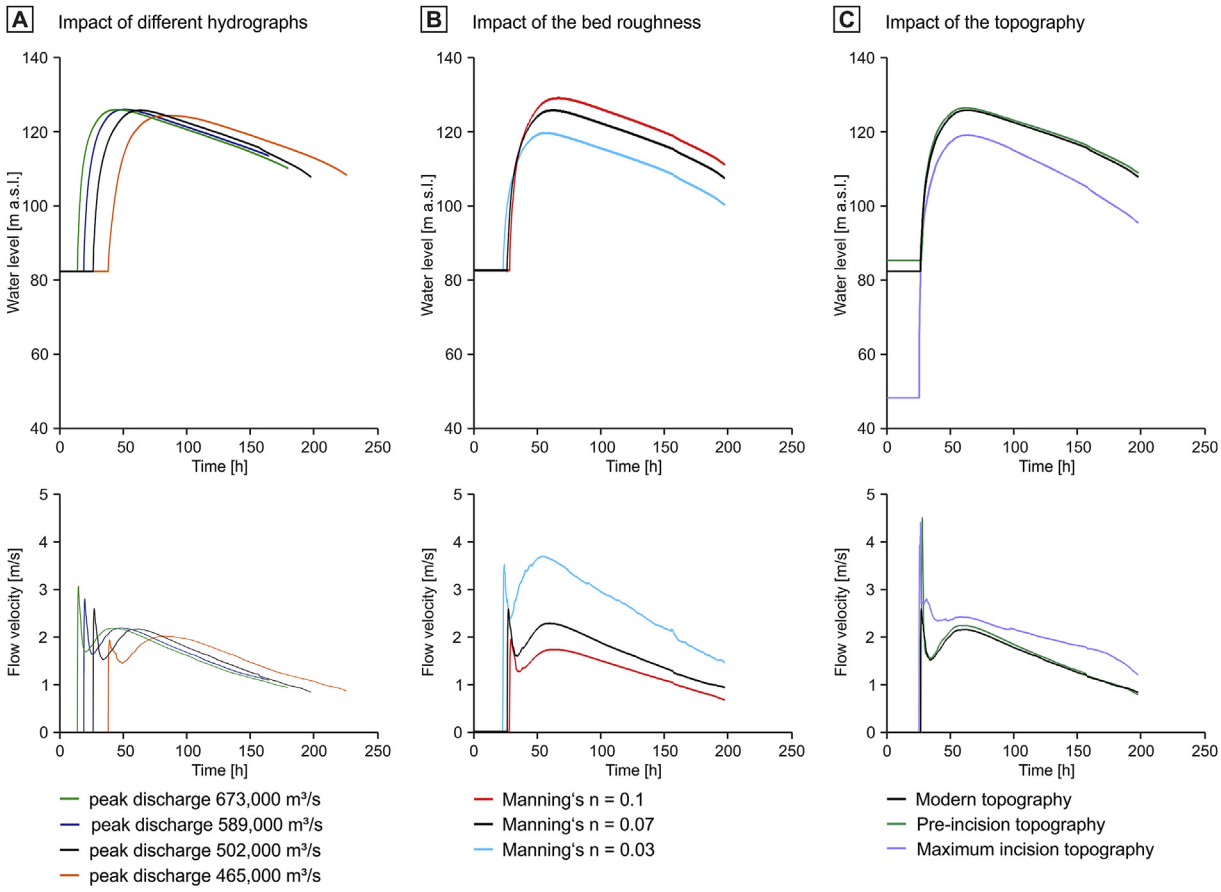

Fig. 7. Sensitivity of the water-level elevation and flow velocity of the simulated flood to different parameters. All data are plotted for observation point P2 (Fig. 5A). The black curves represent the same conditions in all plots. **A)** Impact of different hydrographs (modern topography; Manning's n = 0.07). **B)** Impact of the bed roughness (modern topography; hydrograph: 502,000 m^3s^{-1} peak discharge). **C)** Impact of the basal topography (hydrograph: 502,000 m^3s^{-1} peak discharge; Manning's n = 0.07).

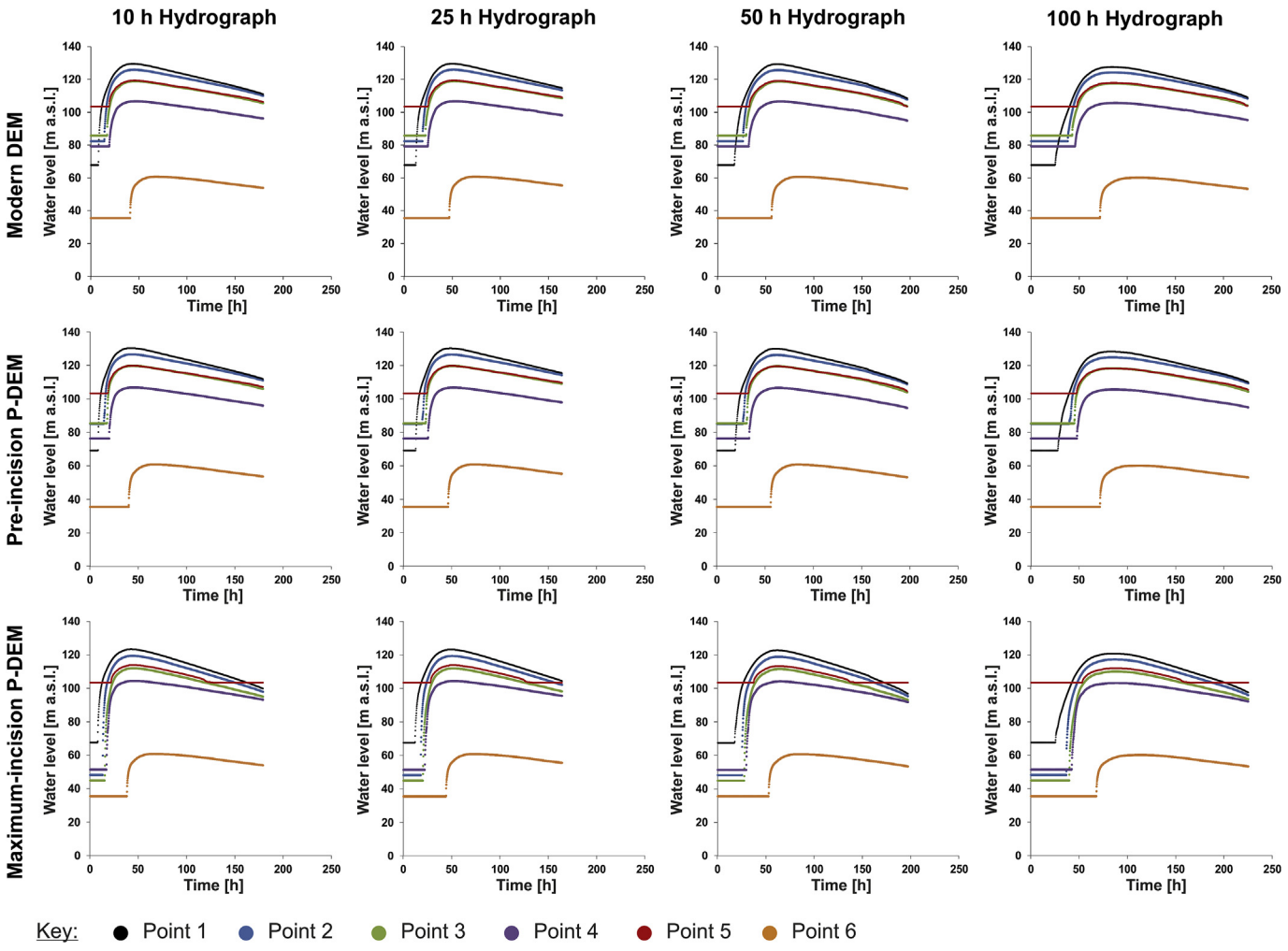

Fig. 8. Plots of the water-level evolution at different locations in the model area during the simulated flood for different hydrographs and basal topographies (Manning's n = 0.07). The locations of the observation points are given in Fig. 5A.

concerned. The match between water levels predicted by the numerical simulations and the elevation of flood-related deposits and streamlined hills is improved by the palaeotopographic model, representing the pre-incision surface (Fig. 10A and B).

5.2. Geomorphologic record in the proximal flood pathway

The mapping of flood-related features indicates a dominance of erosional features along the proximal flood pathway, including large-scale scours, trench-like valleys and streamlined hills (Fig. 3B). The dominance of erosional features is common for outburst floods in topographically confined settings (Kehew and Lord, 1986; Kehew et al., 2009). Furthermore, flood-related deposits are more likely to be subsequently reworked. The distribution of the flood-related features suggests a two-staged sequence of events. During the early stage the flood spread through several valleys between the ice margin and the Groβe Bruch area. The elevation of the streamlined hills and the flood deposits indicates a formation during the early stage, when the water level was high. This is consistent with the numerical flood simulation, which indicates that the necessary high water-level elevations were only attained in the absence of the deep channel of the Groβe Bruch (Fig. 10B). In the later flood stage the flow became focussed through the Groβe Bruch and Oker valleys, leading to enhanced incision, further channelisation and lower water levels in the adjacent areas. The numerical flood simulation indicates high flow velocities and bed-shear stresses in the confined areas, which would allow for deep incision (Fig. 10D and E). Similar two-staged models have been developed for outburst floods, which suggest an initial stage with widespread erosion, including streamlined hills, scours and anastomosing channels, and a subsequent incision of trench-like inner channels (Kehew and Lord, 1986; Carling et al., 2009a; Kehew et al., 2009; Meinsen et al., 2011; Gupta et al., 2017).

5.3. Reconstructing the distal flood pathway

The distal pathway of the simulated flood is mainly controlled by the ice-margin configuration (Fig. 11). Due to the large area and limited data no palaeotopography was reconstructed for the distal flood pathway. West of the Oker valley, remnants of Saalian till display east-west trending elongate geometries and the topography is characterised by shallow, east-west trending depressions (Fig. 11D). These features may relate to erosion by the lake-outburst flood, spreading from the Oker valley towards the west.

The position of the ice-margin during the outburst flood represents a major constraint for the flood pathway but is highly uncertain. West-east to northwest-southeast trending topographic depressions between till plateaus in northwestern Germany and

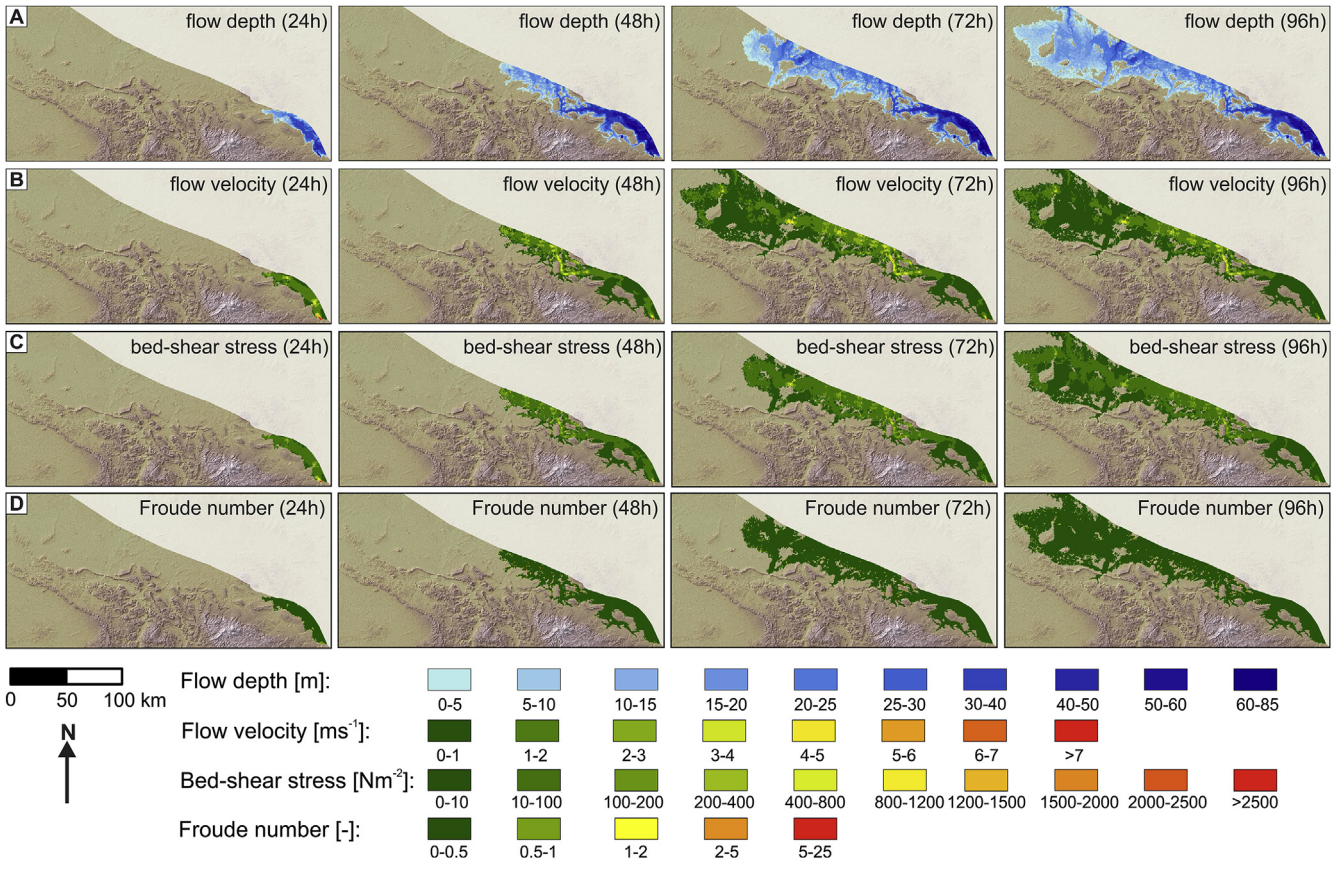

Fig. 9. Maps showing the **A)** flow depth, **B)** flow velocity, **C)** bed-shear stress and **D)** Froude number for an outburst-flood simulation based on the modern topography and a hydrograph, where the peak discharge of 502,000 m^3s^{-1} is reached after 50 h.

the Netherlands act as preferential flood pathways in all tested ice-margin configurations. Further factors to be considered in the reconstruction of the distal flood route are the presence of ice-dammed lakes in the southern North Sea Basin and the central Netherlands and uplift in the area of the glacioisotatic forebulge of the Saalian ice sheet (Lambeck et al., 2006; Busschers et al., 2008; Cohen et al., 2014; Winsemann et al., 2015; De Clercq et al., 2018).

Depending on the ice-margin configuration, the simulations result in three different flood pathways (Figs. 11 and 12). All three pathways correspond to features that have been interpreted as forming part of ice-marginal drainage systems during the older Saalian glaciation (Woldstedt, 1929; Ilies, 1952; Ruegg, 1983; Ter Wee, 1983; Speetzen and Zandstra, 2009; Ehlers et al., 2011; Bregman and Smit, 2012). However, the ice-marginal drainage system during the older Saalian glaciation is poorly constrained.

The southern simulated flood pathway (pathway IIa; Figs. 11A and 12) follows an east-west trending system of glacitectonic ridges and associated basins (Fig. 11D), which were formed during the first advance of the Saalian ice sheet (Meyer, 1987; Van den Berg and Beets, 1987). During the decay of the ice sheet proglacial lakes formed in the excavated glacitectonic basins that were probably partly connected to the larger ice-dammed lake in the southern North Sea Basin (Van den Berg and Beets, 1987; Beets and Beets, 2003; Busschers et al., 2008). The formation of the west-east trending, 20–40 km wide and up to 60 m deep palaeo-Vecht valley has been interpreted as related to the drainage of the proglacial lakes in the Netherlands (Van den Berg and Beets, 1987; Peeters et al., 2015, 2016). The great depth of the palaeo-valley indicates that incision probably occurred during base-level fall when the ice-dammed lake in the southern North Sea Basin drained (Busschers et al., 2008; Peeters et al., 2016). We speculate that the drainage of the large Halle-Leipzig Lake in eastern Germany, releasing more than 200 km^3 of water, may have raised the lake level and triggered the overflow, dam break and subsequent drainage of the ice-dammed lakes in the central Netherlands and North Sea Basin. The North Sea Lake was controlled by a palaeo-high in the Strait of Dover (Fig. 12) (Busschers et al., 2008; Cohen et al., 2014). Bathymetric and seismic data indicate a two-phased breaching of this palaeo-high during the Elsterian/Anglian and Saalian/Wollstonian glaciations (Gupta et al., 2007, 2017; Collier et al., 2015; García-Moreno et al., 2019). Palaeo-channels and fluvial deposits in the southern North Sea Basin indicate that the final breaching occurred during the Saalian glaciation (Busschers et al., 2008; Rijsdijk et al., 2013; Peeters et al., 2015; De Clercq et al., 2018). The final breaching was initiated by increased overspill from the North Sea Lake related to the input of water from the drainage of ice-dammed lakes farther east (Gupta et al., 2017). Overspilling flows from the North Sea Lake were routed through the English Channel palaeo-river towards the North Atlantic, leaving a distinct record in deep marine deposits in the Bay of Biscay (Fig. 12) (Gupta et al., 2007, 2017; Toucanne et al., 2009a, b; Collier et al., 2015). The basal fill of the palaeo-Vecht valley comprises meltwater deposits derived from easterly sources (Peeters et al., 2015, 2016), which might indicate that the valley was initiated by the lake-outburst floods from northwestern and central Germany and subsequently acted as a major meltwater-drainage pathway. Luminescence ages of the overlying fluvial valley fill range from 143 to 119 ka (Peeters et al., 2016), pointing to a deposition during the middle or younger Saalian glaciation. From

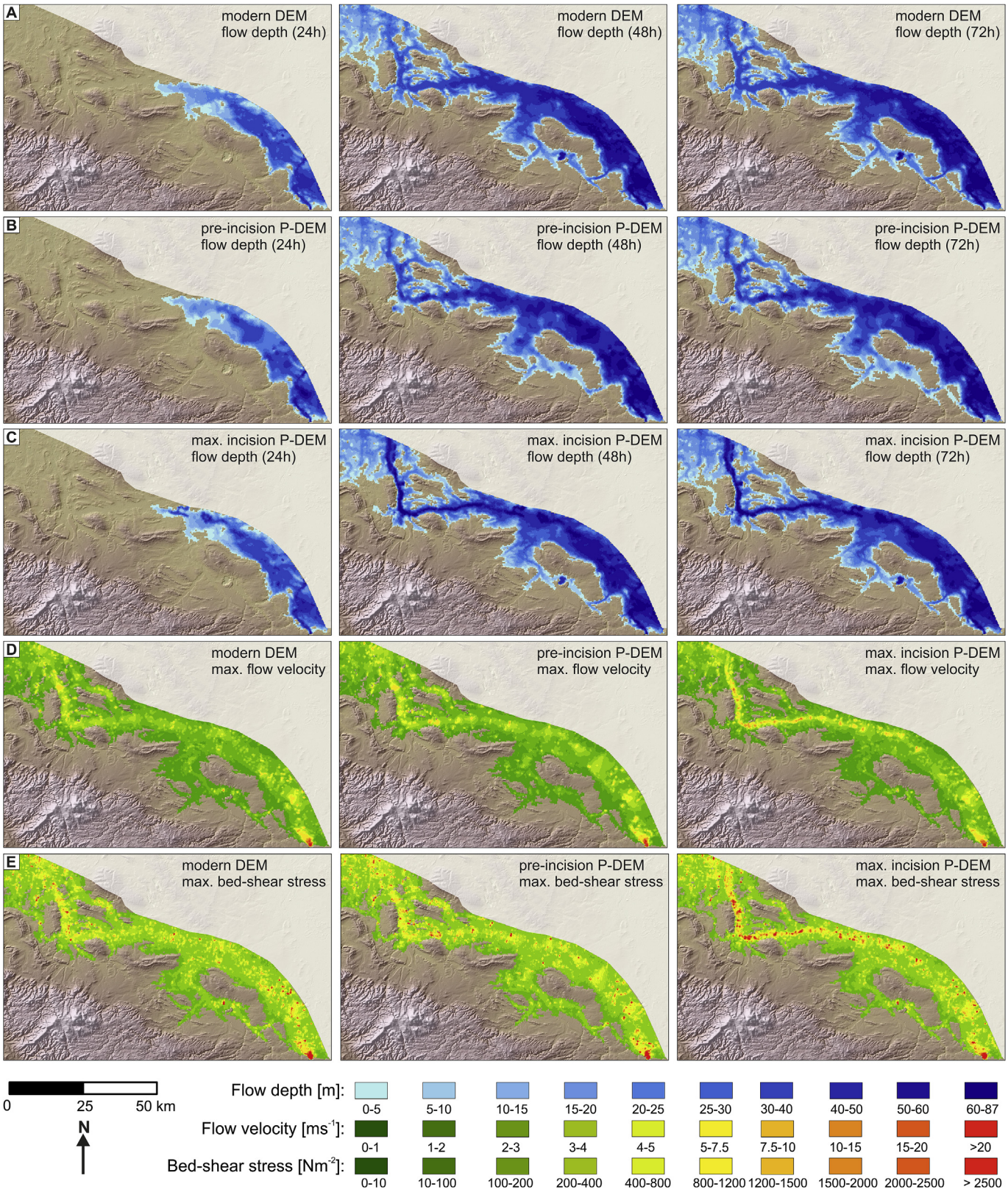

Fig. 10. Comparison of the simulation results. All simulations were run with a hydrograph, where the peak discharge of 502,000 m^3s^{-1} is reached after 50 h. **A)** Flow depth, using the modern topography. **B)** Flow depth, using the pre-incision palaeotopography. **C)** Flow depth, using the maximum incision palaeotopography. **D)** Maximum flow velocity in simulations using the modern topography (left), pre-incision palaeotopography (centre) and maximum incision palaeotopography (right). **E)** Maximum bed-shear stress in simulations using the modern topography (left), pre-incision palaeotopography (centre) and maximum incision palaeotopography (right).

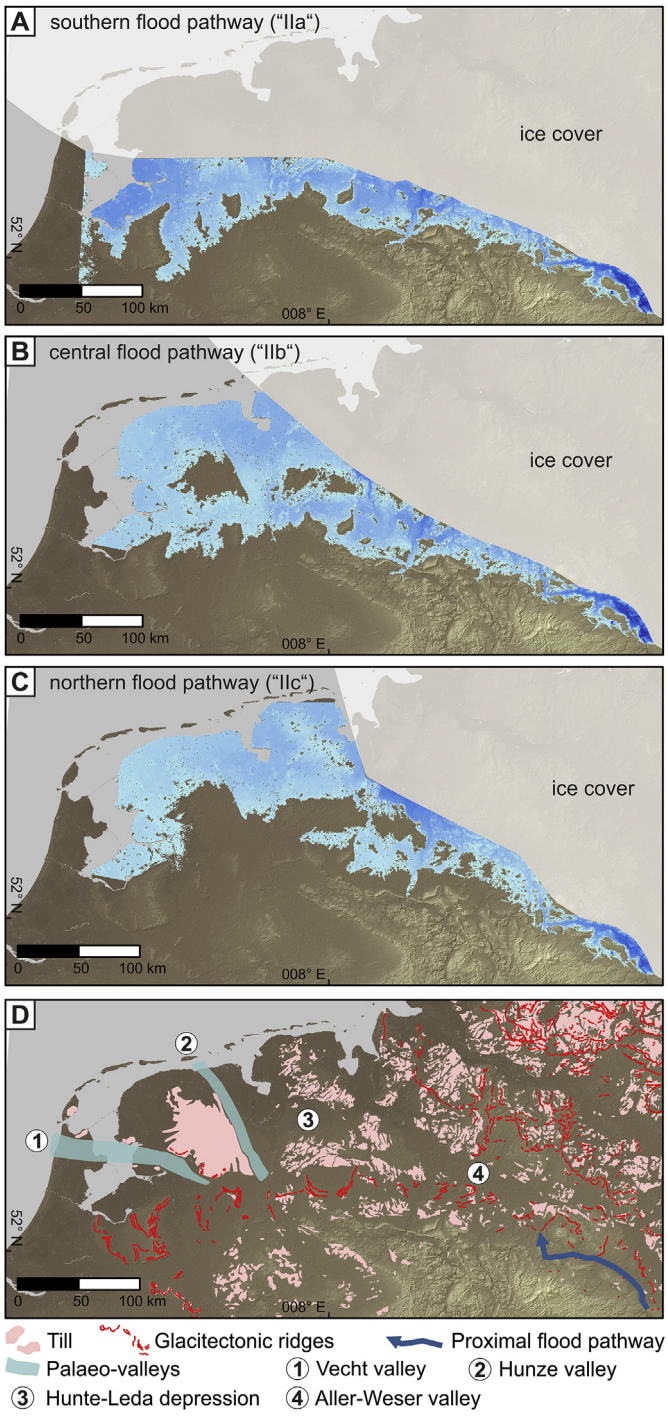

Fig. 11. Simulated flood pathways controlled by the ice-margin configuration. **A)** Southern flood pathway ("IIa"). **B)** Central flood pathway ("IIb") **C)** Northern flood pathway ("IIc") **D)** Distribution of till and glacitectonic ridges and location of palaeo-valleys along the potential flood pathways in northwestern Germany and the Netherlands (compiled from Pierik, 2010; Ehlers et al., 2011; Peeters et al., 2015; BGR, 2018).

the latest Saalian to the middle Weichselian the palaeo-valley was occupied by the River Rhine (Van den Berg and Beets, 1987; Peeters et al., 2015, 2016).

The central simulated flood pathway (pathway II; Figs. 11B and 12) shows a splitting of the outburst flood, which partly follows the southern pathway along the glacitectonic ridges and partly flows to the northwest and west through the Hunte-Leda depression and probably continuing through the palaeo-Hunze valley in the northeastern Netherlands (cf., Van den Berg and Beets, 1987). The northern simulated flood pathway (pathway IIc; Figs. 11C and 12) follows the course of the River Oker into the Aller-Weser valley.

The southern pathway (pathway IIa; Figs. 11A and 12) seems to be the most likely flood pathway, while both pathways farther north (pathways IIb and IIc; Fig. 11B and C, 12) seem less likely. The presence of a continuous till plateau, partly bearing mega-scale glacial lineations related to the first older Saalian ice advance (Lang et al., 2018), is hard to reconcile with potential flood-related erosion in the central flood pathway (pathway IIb; Figs. 11B and 12). The northern pathway (pathway IIc; Figs. 11C and 12) requires an unrealistic ice-margin configuration with an advanced stage of ice-sheet decay in the northwest to open the potential drainage route, while an extensive ice margin in the southeast is required to provide the ice dam prior to the outburst flood.

5.4. Impact of the outburst flood on the drainage system

The retreat of the ice margin and the drainage of ice-marginal lakes led to a successive opening of the meltwater-drainage system, which was largely blocked during the maximum extent of the older Saalian ice sheet (Figs. 2A and 12). The drainage of the Halle-Leipzig Lake strongly modified the regional drainage network due to the incision of channels that crosscut pre-existing drainage divides. In the proximal flood pathway the incision of the Groβe Bruch valley established a west-east trending connection, crossing the regional drainage divide between the Rivers Oker and Saale (Fig. 3B). The distribution of early Saalian fluvial deposits in the study area (Weymann et al., 2005) points to the existence of a pronounced drainage divide between those rivers prior to the Saalian glaciation. The west-east trending topographic depressions in northwestern Germany and the Netherlands probably also relate to the glacial lake-outburst flood and mark the distal flood pathway.

The modification of the drainage network by the glacial-lake outburst flood strongly impacted the drainage of meltwater during the subsequent ice-sheet decay. During the retreat of the Saalian ice-sheet from the study area, the Groβe Bruch and Oker valleys drained the ice sheet east of the River Saale (Schulz, 1962; Ruske, 1963, 1973; Ehlers et al., 2011). The channels initiated by the lake-outburst flood became a crucial part of the ice-marginal drainage system, receiving meltwater from a substantial part of the decaying Saalian ice sheet. The drainage route continued towards the North Sea Basin (Fig. 12), probably following the same route as the outburst flood that established the drainage system until further ice-margin retreat re-opened the drainage pathways towards the north.

6. Conclusions

The formation and drainage of ice-dammed lakes along the southwestern margin of the Middle Pleistocene (Saalian) Fennoscandian ice sheet had a major impact on the regional drainage network and the landscape evolution. Glacial lake-outburst floods occurred in response to the opening of spillways during ice-margin retreat.

The largest individual glacial lake-outburst flood occurred when the ~224 km^3 Halle-Leipzig Lake cataclysmically drained after the failure of an ice dam in the Saale gorge. The reconstructed outlet hydrographs indicate peak discharges between 465,000 and 673,000 m^3s^{-1}. The outburst flood spread towards the northwest and inundated large parts of northwestern Germany and the Netherlands. Flood-related erosional and depositional features in

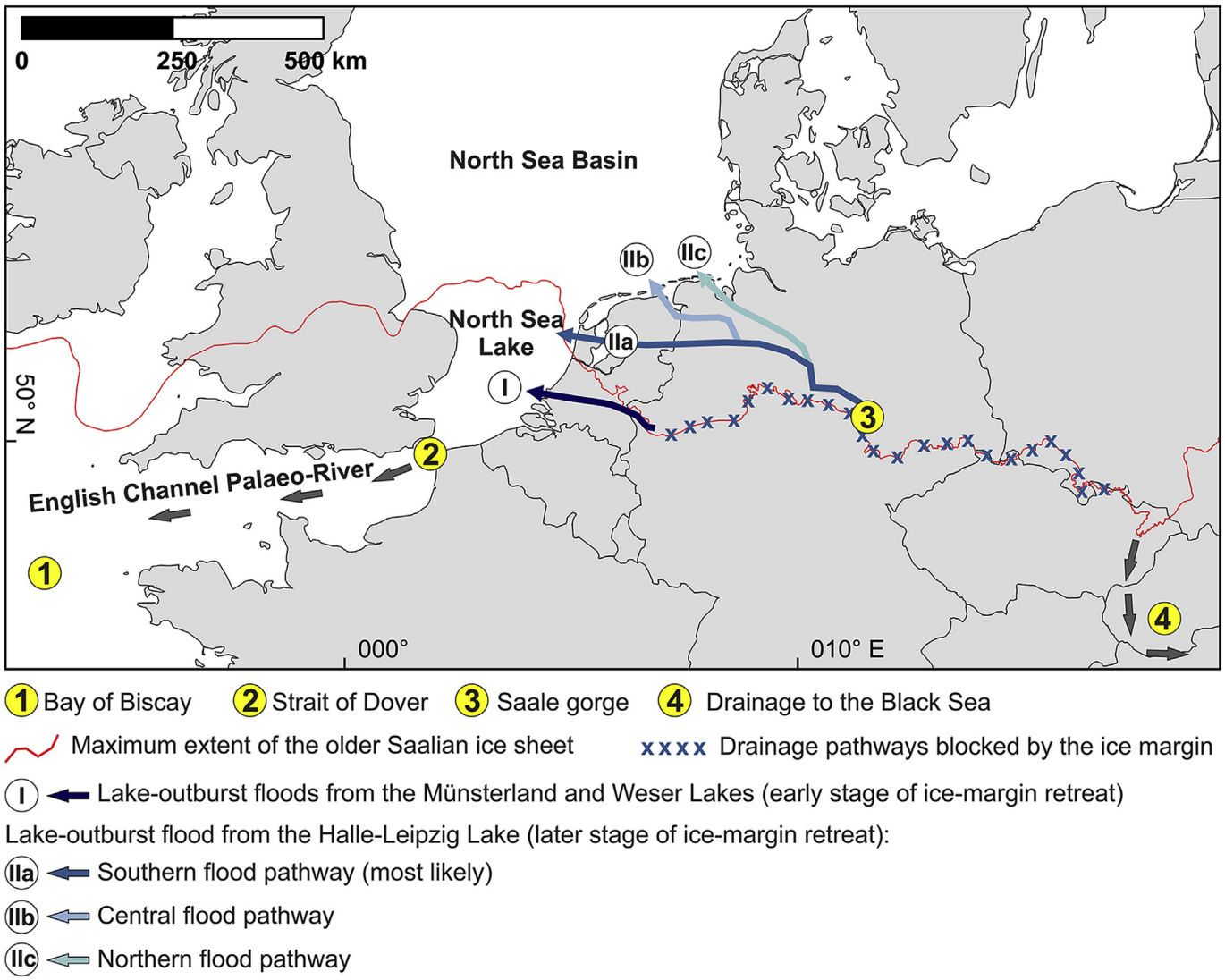

Fig. 12. Overview of the meltwater-drainage pathways of the Middle Pleistocene older Saalian glaciation. During the maximum ice-sheet extent all meltwater-drainage pathways up to the drainage divide between the Atlantic and the Black Sea in eastern Poland were blocked. "I" indicates the drainage pathway of successive floods from the Weser and Münsterland Lakes (Meinsen et al., 2011; Winsemann et al., 2016). "II" indicates the potential drainage pathways of the flood from the Halle-Leipzig Lake. "IIa" indicates the most likely northern pathway along glacitectonic basins and the palaeo-Vecht valley. "IIb" is the central pathway through the Hunte-Leda depression and the palaeo-Hunze valley. "IIc" is the northern pathway through the Aller-Weser valley.

the proximal flood pathway (within ~150 km from the outlet) include large-scale scours, trench-like channels, streamlined hills, giant bars and run-up deposits. Based on the field evidence a two-stage model is proposed. In the early stage the outburst flood spread more widely and was confined by northwest-southeast trending structural valleys. Streamlined hills, isolated scours and giant bars probably relate to this early flood stage. During the later flood stage trench-like valleys were incised. The channelisation of the flow through these valleys during the later flood stage led to the further deepening of the valleys.

The numerical flow simulation of the spreading of the outburst flood indicates flow depths of up to 87 m, flow velocities of up to 7 ms^{-1} and peaks of the bed-shear stress of up to 2500 Nm^{-2}. The spreading and flow dynamics of outburst floods are strongly controlled by the underlying topography. To account for the effect of the topography the palaeotopography prior to the outburst flood and during the maximum flood-related incision, respectively, were reconstructed. The simulation of the outburst flood was conducted based on the modern digital elevation model and on the palaeotopographic models. The different simulations display some divergence in peak flow depths, velocities and bed-shear stresses. The observations from the different simulations support the interpretation of a two-staged flood model, where an earlier stage of wider and deeper inundation followed by a later stage of strong channelisation. The palaeotopographic models thus improve the consistency between the field evidence and simulation results.

The glacial-lake outburst flood most likely impacted the drainage pathway of meltwater during the subsequent ice-sheet decay. The proximal trench-like channels initiated by the lake-outburst flood became a crucial part of the ice-marginal drainage system and conveyed meltwater from a substantial part of the decaying Saalian ice sheet. Distally, the outburst flood probably followed an east-west route through northwestern Germany and the central Netherlands into the ice-dammed lakes in the central Netherlands and southern North Sea Basin. The added water volume might have led to the overspill and drainage of the proglacial lakes in the central Netherlands and the North Sea Lake and the breaching of the Strait of Dover in a chain reaction, eventually

opening an east-west trending meltwater-drainage pathway along the southwestern margin of the decaying ice sheet.

Acknowledgements

Funding for this study was provided in the framework of the "Wege in die Forschung" program by Leibniz Universität Hannover (project title: "Mittelpleistozäne Megafluten in Norddeutschland: Auswirkungen und Magnituden"; Grant No. II-05-2014-05). Additional funding was provided by the Academy of Finland Strategic Research Council project "COMBAT" (Grant No. 293389). R. Pioch, J. Sievers and T. Steinbrecher are thanked for GIS work. The hill-shaded relief maps were produced using Copernicus data and information funded by the European Union (EU-DEM layers). Borehole data were generously provided by Niedersächsisches Landesamt für Bergbau, Energie und Geologie (LBEG). Fugro is acknowledged for providing GeODin, which was used for borehole-data management. Constructive reviews by J. Herget and an anonymous reviewer are highly appreciated and helped to improve our manuscript.

Appendix A. Supplementary data

Supplementary data to this article can be found online at https://doi.org/10.1016/j.quascirev.2019.02.018.

References

Alho, P., Russell, A.J., Carrivick, J.L., Käyhkö, J., 2005. Reconstruction of the largest Holocene jökulhlaup within Jökulsá á Fjöllum, NE Iceland. Quat. Sci. Rev. 24, 2319–2334.
Alho, P., Baker, V.R., Smith, L.N., 2010. Paleohydraulic reconstruction of the largest Glacial Lake Missoula draining(s). Quat. Sci. Rev. 29, 3067–3078.
Baker, V.R., 1973. Paleohydrology and Sedimentology of Lake Missoula Flooding in Eastern Washington, vol. 144. Geological Society of America Special Paper, Boulder, CO, pp. 1–7.
Baker, V.R., 2009. Channelled scabland morphology. In: Burr, D.M., Carling, P.A., Baker, V.R. (Eds.), Megaflooding on Earth and Mars. Cambridge University Press, Cambridge, pp. 65–77.
Beeson, J.W., Goldfinger, C., Fortin, W.F., 2017. Large-scale modification of submarine geomorphic features on the Cascadia accretionary wedge caused by catastrophic flooding events. Geosphere 13, 1713–1728.
Beets, C.J., Beets, D.J., 2003. A high resolution stable isotope record of the penultimate deglaciation in lake sediments below the city of Amsterdam, The Netherlands. Quat. Sci. Rev. 22, 195–207.
Beets, D.J., Meijer, T., Beets, C.J., Cleveringa, P., Laban, C., Van der Spek, A.J.F., 2005. Evidence for a middle Pleistocene glaciation of MIS 8 age in the southern North sea. Quat. Int. 133, 7–19.
Best, J.L., Ashworth, P.J., 1997. Scour in large braided rivers and the recognition of sequence stratigraphic boundaries. Nature 387, 275.
Best, J.L., Roy, A.G., 1991. Mixing-layer distortion at the confluence of channels of different depth. Nature 350, 411.
Betz, D., Führer, F., Greiner, G., Plein, E., 1987. Evolution of the lower saxony basin. Tectonophysics 137, 127–170.
BGR, 2018. Geological Mapof Germany, 1:1,000,000. Bundesanstalt für Geowissenschaften, Hannover.
Bohorquez, P., Carling, P.A., Herget, J., 2016. Dynamic simulation of catastrophic late Pleistocene glacial-lake drainage, Altai Mountains, central Asia. Int. Geol. Rev. 58, 1795–1817.
Brandes, C., Pollok, L., Schmidt, C., Wilde, V., Winsemann, J., 2012. Basin modelling of a lignite-bearing salt rim syncline: insights into rim syncline evolution and salt diapirism in NW Germany. Basin Res. 24, 699–716.
Brandes, C., Schmidt, C., Tanner, D.C., Winsemann, J., 2013. Paleostress pattern and salt tectonics within a developing foreland basin (northwestern Subhercynian Basin, northern Germany). Int. J. Earth Sci. 102, 2239–2254.
Bregman, E.P.H., Smit, F.W.H., 2012. Genesis of the Hondsrug, a Saalian Megaflute, Drenthe, the Netherlands. European Geopark de Hondsrug, Borger, p. 123.
Brunner, G.W., 2016. HEC-RAS, River Analysis System Hydraulic Reference Manual, CPD 69. US Army Corps of Engineers Hydraulic Engineering Center (HEC), Davis, p. 538.
Busschers, F.S., Van Balen, R.T., Cohen, K.M., Kasse, C., Weerts, H.J., Wallinga, J., Bunnik, F.P., 2008. Response of the Rhine-Meuse fluvial system to Saalian ice-sheet dynamics. Boreas 37, 377–398.
Carling, P.A., 2013. Freshwater megaflood sedimentation: what can we learn about generic processes? Earth Sci. Rev. 125, 87–113.
Carling, P.A., Kirkbride, A.D., Parnachov, S., Borodavko, P.S., Berger, G.W., 2002. Late Quaternary catastrophic flooding in the Altai mountains of south-central Siberia: a synoptic overview and an introduction to flood deposit sedimentology. In: Martini, P.I., Baker, V.R., Garzon, G. (Eds.), Flood and Megaflood Processes and Deposits: Recent and Ancient Examples. Special Publications of the International Association of Sedimentologists 32. Blackwell Science, Oxford, pp. 17–35.
Carling, P.A., Burr, D.M., Johnsen, T.F., Brennand, T.A., 2009a. A review of open-channel megaflood depositional landforms on Earth and Mars. In: Burr, D.M., Carling, P.A., Baker, V.R. (Eds.), Megaflooding on Earth and Mars. Cambridge University Press, Cambridge, pp. 33–49.
Carling, P.A., Herget, J., Lanz, J.K., Richardson, K., Pacifici, A., 2009b. Channel-scale erosional bedforms in bedrock and in loose granular material: character, processes and implications. In: Burr, D.M., Carling, P.A., Baker, V.R. (Eds.), Megaflooding on Earth and Mars. Cambridge University Press, Cambridge, pp. 13–32.
Carling, P., Villanueva, I., Herget, J., Wright, N., Borodavko, P., Morvan, H., 2010. Unsteady 1-D and 2-D hydraulic models with ice-dam break for Quaternary megafloods, Altai Mountains, southern Siberia. Glob. Planet. Chang. 70, 24–34.
Carrivick, J.L., 2010. Dam break–outburst flood propagation and transient hydraulics: a geosciences perspective. J. Hydrol. 380, 338–355.
Caspers, G., Jordan, H., Merkt, J., Meyer, K.-D., Müller, H., Streif, H., 1995. Niedersachsen. In: Benda, L. (Ed.), Das Quartär Deutschlands. Bornträger, Berlin, pp. 23–58.
Cohen, K.M., Gibbard, P.L., Weerts, H.J.T., 2014. North Sea palaeogeographical reconstructions for the last 1 Ma. Neth. J. Geosci. 93, 7–29.
Collier, J.S., Oggioni, F., Gupta, S., García-Moreno, D., Trentesaux, A., De Batist, M., 2015. Streamlined islands and the English Channel megaflood hypothesis. Glob. Planet. Chang. 135, 190–206.
Curry, B.B., Hajic, E.R., Clark, J.A., Befus, K.M., Carrell, J.E., Brown, S.E., 2014. The Kankakee torrent and other large meltwater flooding events during the last deglaciation, Illinois, USA. Quat. Sci. Rev. 90, 22–36.
Dahlgrün, F., 1939. Erläuterungen zur geologischen Karte von Preussen und benachbarten deutschen Ländern, 1:25000, Blatt 3928 Salzgitter. Preußische Geologische Landesanstalt, Berlin, p. 92.
De Clercq, M., Missiaen, T., Wallinga, J., Zurita Hurtado, O., Versendaal, A., Mathys, M., De Batist, M., 2018. A well-preserved eemian incised-valley fill in the southern North Sea Basin, Belgian continental shelf-coastal plain: implications for northwest european landscape evolution. Earth Surf. Process. Landforms 43, 1913–1942.
Denlinger, R.P., O'Connell, D.R.H., 2010. Simulations of cataclysmic outburst floods from Pleistocene glacial lake Missoula. Geol. Soc. Am. Bull. 122, 678–689.
Ehlers, J., 1990. Reconstructing the dynamics of the north-west European Pleistocene ice sheets. Quat. Sci. Rev. 9, 71–83.
Ehlers, J., Grube, A., Stephan, H.J., Wansa, S., 2011. Pleistocene glaciations of North Germany – new results. In: Ehlers, J., Gibbard, P.L., Hughes, P.D. (Eds.), Quaternary Glaciations – Extent and Chronology – A Closer Look. Developments in Quaternary Science 15. Elsevier, Amsterdam, pp. 149–162.
Eissmann, L., 1975. Das Quartär der Leipziger Tieflandsbucht und angrenzender Gebiete um Saale und Elbe – modell einer Landschaftsentwicklung am Rand der europäischen Kontinentalvereisung. Schriftenreihe geologischer Wissenschaften 2, 1–263.
Eissmann, L., 2002. Quaternary geology of eastern Germany (saxony, saxon-anhalt, south brandenburg, thüringia), type area of the elsterian and saalian stages in Europe. Quat. Sci. Rev. 21, 1275–1346.
Feldmann, L., Groetzner, J.-P., Weymann, H.-J., 2001. Zur pleistozänen Geschichte des „Großen Bruch" im nördlichen Harzvorland. Geol. Beitraege Hann. 2, 127–137.
Froese, D.G., Smith, D.G., Westgate, J.A., Ager, T.A., Preece, S.J., Sandhu, A., Enkin, R.J., Weber, F., 2003. Recurring middle Pleistocene outburst floods in east-central Alaska. Quat. Res. 60, 50–62.
García-Moreno, D., Gupta, S., Collier, J.S., Oggioni, F., Vanneste, K., Trentesaux, A., Verbeeck, K., Versteeg, W., Jomard, H., Camelbeeck, T., De Batist, M., 2019. Middle-Late Pleistocene landscape evolution of the Dover Strait inferred from buried and submerged erosional landforms. Quat. Sci. Rev. 203, 209–232.
Gassert, D., 1975. Stausee- und Rinnenbildung an den südlichsten Eisrandlagen in Norddeutschland. Wurzbg. Geogr. Arb. 43, 55–65.
Gupta, S., Collier, J.S., Palmer-Felgate, A., Potter, G., 2007. Catastrophic flooding origin of shelf valley systems in the English Channel. Nature 448, 342–345.
Gupta, S., Collier, J.S., Garcia-Moreno, D., Oggioni, F., Trentesaux, A., Vanneste, K., De Batst, M., Camelbeeck, T., Potter, G., van Vliet-Lanoë, B., Arthur, J.C., 2017. Two-stage opening of the dover strait and the origin of island britain. Nat. Commun. 8 https://doi.org/10.1038/ncomms15101.
Hall, A.M., Migoń, P., 2010. The first stages of erosion by ice sheets: evidence from central Europe. Geomorphology 123, 349–363.
Herget, J., 1998. Temporäre Entwässerungsbahnen am Südrand der Westfälischen Tieflandsbucht – ein Szenario. In: Glatthaar, D., Herget, J. (Eds.), Physische Geographie und Landeskunde – Festschrift für Herbert Liedtke. Bochumer Geographische Arbeiten, Sonderreihe 13. Geographisches Institut, Bochum, pp. 23–30.
Herget, J., 2002. Sedimentary traces as indicator of temporary ice-marginal channels in the Westphalian Bight, Germany. In: Martini, P.I., Baker, V.R., Garzon, G. (Eds.), Flood and Megaflood Processes and Deposits: Recent and Ancient Examples. Special Publications of the International Association of Sedimentologists 32. Blackwell Science, Oxford, pp. 283–290.
Herget, J., 2005. Reconstruction of Pleistocene Ice-Dammed Lake Outburst Floods in the Altai-Mountains, Siberia, vol. 386. Geological Society of America Special

Paper, pp. 1–118.
Herget, J., Schütte, F., Klosterhalfen, A., 2015. Empirical modelling of outburst flood hydrographs. Zeitschrift für Geomorphologie, Supplementary Issues 59, 177–198.
Hinze, C., Höfle, H.-C., Jordan, H., Mengeling, H., Meyer, K.-D., Rohde, P., Streif, H., 1995. Quartärgeologische Übersichtskarte von Niedersachsen und Bremen, 1: 500,000. Niedersächsisches Landesamt für Bodenforschung.
Hoyal, D.C.J.D., Van Wagoner, J.C., Adair, N.L., Deffenbaugh, M., Li, D., Sun, T., Huh, C., Giffin, D.E., 2003. Sedimentation from jets: a depositional model for clastic deposits of all scales and environments. Search and Discovery. Article # 40082.
Ilies, H., 1952. Eisrandlagen und eiszeitliche Entwässerung in der Umgebung von Bremen. Abhandlungen des naturwissenschaftlichen Vereins zu Bremen 33, 19–56.
Junge, F.W., 1998. Die Bändertone Mitteldeutschlands und angrenzender Gebiete. Altenbg. Naturwiss. Forsch. 9, 1–210.
Junge, F.W., Böttger, T., Siegert, C., 1999. Die Stauseesedimente des Bruckdorfer Horizontes: ergebnis der Eisrandoszillation des saaleglazialen skandinavischen Inlandeises in Mitteldeutschland. Mauritiana 17, 257–276.
Kars, R.H., Busschers, F.S., Wallinga, J., 2012. Validating post IR-IRSL dating on K-feldspars through comparison with quartz OSL ages. Quat. Geochronol. 12, 74–86.
Kehew, A.E., Lord, M.L., 1986. Origin and large-scale erosional features of glacial-lake spillways in the northern Great Plains. Geol. Soc. Am. Bull. 97, 162–177.
Kehew, A.E., Lord, M.L., Kozlowski, A.L., Fisher, T.G., 2009. Proglacial megaflooding along the margins of the laurentide ice sheet. In: Burr, D.M., Carling, P.A., Baker, V.R. (Eds.), Megaflooding on Earth and Mars. Cambridge University Press, Cambridge, pp. 104–127.
Kenzler, M., Tsukamoto, S., Meng, S., Frechen, M., Hüneke, H., 2017. New age constraints from the SW Baltic Sea area – implications for Scandinavian Ice Sheet dynamics and palaeo-environmental conditions during MIS 3 and early MIS 2. Boreas 46, 34–52.
Klostermann, J., 1992. Das Quartär der Niederrheinischen Bucht – Ablagerungen der letzten Eiszeit am Niederrhein. Geologisches Landesamt Nordrhein-Westfalen, Krefeld, p. 200.
Knoth, W., 1964. Zur Kenntnis der pleistozänen Mittelterrassen der Saale und Mulde nördlich von Halle. Geologie 13, 598–616.
Koch, R., 2015. Ergebnisse von geologischen Kartierbohrungen des LBEG im Großen Bruch (nördliches Harzvorland). LUNG-Heft 01/2015, pp. 93–95.
Kockel, F., 1991. Die Struktur im Untergrund des Braunschweigischen Landes. Geol. Jahrb. 127, 391–404.
Komar, P.D., 1983. Shapes of streamlined islands on Earth and Mars: experiments and analyses of the minimum-drag form. Geology 11, 651–654.
Komatsu, G., Baker, V.R., Arzhannikov, S.G., Gallagher, R., Arzhannikova, A.V., Murana, A., Oguchi, T., 2016. Catastrophic flooding, palaeolakes, and late Quaternary drainage reorganization in northern Eurasia. Int. Geol. Rev. 58, 1693–1722.
Lambeck, K., Purcell, A., Funder, S., Kjær, K.H., Larsen, E., Moller, P., 2006. Constraints on the Late Saalian to early Middle Weichselian ice sheet of Eurasia from field data and rebound modelling. Boreas 35, 539–575.
Lang, J., Winsemann, J., 2013. Lateral and vertical facies relationships of bedforms deposited by aggrading supercritical flows: from cyclic steps to humpback dunes. Sediment. Geol. 296, 36–54.
Lang, J., Winsemann, J., Steinmetz, D., Polom, U., Pollok, L., Böhner, U., Serangeli, J., Brandes, C., Hampel, A., Winghart, S., 2012. The Pleistocene of Schöningen, Germany: a complex tunnel valley fill revealed from 3D subsurface modelling and shear wave seismics. Quat. Sci. Rev. 39, 86–105.
Lang, J., Lauer, T., Winsemann, J., 2018. New age constraints for the Saalian glaciation in northern central Europe: implications for the extent of ice sheets and related proglacial lake systems. Quat. Sci. Rev. 180, 240–259.
Lauer, T., Weiss, M., 2018. Timing of the Saalian-and Elsterian glacial cycles and the implications for Middle Pleistocene hominin presence in central Europe. Sci. Rep. 8, 5111.
Litt, T., Behre, K.-E., Meyer, K.-D., Stephan, H.-J., Wansa, S., 2007. Stratigraphische Begriffe für das Quartär des norddeutschen Vereisungsgebietes. E&G Quaternary Science Journal 56, 7–65.
Lohr, T., Krawczyk, C.M., Tanner, D.C., Samiee, R., Endres, H., Oncken, O., Trappe, H., Kukla, P.A., 2007. Strain partitioning due to salt: insights from interpretation of a 3D seismic data set in the NW German Basin. Basin Res. 19, 579–597.
Look, E.-R., 1984. Geologie und Bergbau im Braunschweiger Land. Geol. Jahrb. 78, 1–467.
Lüthgens, C., Böse, M., Krbetschek, M., 2010. On the age of the young morainic morphology in the area ascribed to the maximum extent of the Weichselian glaciation in north-eastern Germany. Quat. Int. 222, 72–79.
Mangerud, J., Jakobsson, M., Alexanderson, H., Astakhov, V., Clarke, G.K.C., Henriksen, M., Hjort, C., Krinner, G., Lunkka, J.-P., Möller, P., Murray, A., Nikolskaya, O., Saarnisto, M., Svendsen, J.I., 2004. Ice-dammed lakes and rerouting of the drainage of northern Eurasia during the Last Glaciation. Quat. Sci. Rev. 23, 1313–1332.
Marcinkowski, B., Cepek, A.G., 1982. Osterwiek 2262. Lithofazieskarten Quartär 1: 50,000. Zentrales Geologisches Institut, Berlin.
Marcinkowski, B., Cepek, A.G., Rosenberger, G., 1973. Magdeburg Süd 2264. Lithofazieskarten Quartär 1:50,000. Zentrales Geologisches Institut, Berlin.
Marcinkowski, B., Rosenberger, G., Cepek, A.G., Steinmüller, A., 1982. Bernburg 2364. Lithofazieskarten Quartär 1:50,000. Zentrales Geologisches Institut, Berlin.
Margold, M., Jansen, J.D., Codilean, A.T., Preusser, F., Gurinov, A.L., Fujioka, T., Fink, D., 2018. Repeated megafloods from glacial lake vitim, Siberia, to the arctic ocean over the past 60,000 years. Quat. Sci. Rev. 187, 41–61.
Marren, P.M., Schuh, M., 2009. Criteria for identifying jökulhlaups deposits in the sedimentary record. In: Burr, D.M., Carling, P.A., Baker, V.R. (Eds.), Megaflooding on Earth and Mars. Cambridge University Press, Cambridge, pp. 225–242.
Meinsen, J., Winsemann, J., Weitkamp, A., Landmeyer, N., Lenz, A., Dölling, A., 2011. Middle Pleistocene (Saalian) lake outburst floods in the Münsterland Embayment (NW Germany): impacts and magnitudes. Quat. Sci. Rev. 30, 2597–2625.
Meyer, K.-D., 1987. Ground and end moraines in lower saxony. In: van der Meer, J.J.M. (Ed.), Tills and Glaciotectonics. Balkema, Rotterdam, pp. 197–204.
Miyamoto, H., Komatsu, G., Baker, V.R., Dohm, J.M., Ito, K., Tosaka, H., 2007. Cataclysmic scabland flooding: insights from a simple depth-averaged numerical model. Environ. Model. Softw 22, 1400–1408.
Miyamoto, H., Itoh, K., Komatsu, G., Baker, V.R., Dohm, J.M., Tosaka, H., Sasaki, S., 2006. Numerical simulations of large-scale cataclysmic floodwater: a simple depth-averaged model and an illustrative application. Geomorphology 76, 179–192.
Moreau, J., Huuse, M., Janszen, A., van der Vegt, P., Gibbard, P.L., Moscariello, A., 2012. The glaciogenic unconformity of the southern North Sea. In: Huuse, M., Redfern, J., Le Heron, D.P., Dixon, R.J., Moscariello, A., Craig, J. (Eds.), Glaciogenic Reservoirs. Geological Society Special Publication, vol. 368. Geological Society, London, pp. 99–110.
Patton, P.C., Baker, V.R., 1978. New evidence for pre-Wisconsin flooding in the channeled scabland of eastern Washington. Geology 6, 567–571.
Peeters, J., Busschers, F.S., Stouthamer, E., 2015. Fluvial evolution of the Rhine during the last interglacial-glacial cycle in the southern North Sea basin: a review and look forward. Quat. Int. 357, 176–188.
Peeters, J., Busschers, F.S., Stouthamer, E., Bosch, J.H.A., Van den Berg, M.W., Wallinga, J., Versendaal, A.J., Bunnik, F.P.M., Middelkoop, H., 2016. Sedimentary architecture and chronostratigraphy of a late Quaternary incised-valley fill: a case study of the late Middle and Late Pleistocene Rhine system in The Netherlands. Quat. Sci. Rev. 131, 211–236.
Perkins, A.J., Brennand, T.A., 2014. Refining the pattern and style of Cordilleran Ice Sheet retreat: palaeogeography, evolution and implications of late glacial ice-dammed lake systems on the southern Fraser Plateau, British Columbia, Canada. Boreas 44, 319–342.
Pierik, H.J., 2010. An Integrated Approach to Reconstruct the Saalian Glaciation. Utrecht University, unpublished MSc thesis, p. 142.
Reinecke, V., 2006. Untersuchungen zur jungpleistozänen Reliefentwicklung und Morphodynamik im nördlichen Harzvorland. Aachen. Geogr. Arb. 43, 1–170.
Rijsdijk, K.F., Kroon, I.C., Meijer, T., Passchier, S., van Dijk, T.A.G.P., Bunnik, F.P.M., Janse, A.C., 2013. Reconstructing Quaternary Rhine-Meuse dynamics in the southern North Sea: architecture, seismo-lithofacies associations and malacological biozonation. J. Quat. Sci. 28, 453–466.
Rosenberger, G., Cepek, A.G., Marcinkowski, B., 1973. Halberstadt 2263. Lithofazieskarten Quartär 1:50,000. Zentrales Geologisches Institut, Berlin.
Rosenwinkel, S., Landgraf, A., Schwanghart, W., Volkmer, F., Dzhumabaeva, A., Merchel, S., Rugel, G., Preusser, F., Korup, O., 2017. Late Pleistocene outburst floods from issyk kul, Kyrgyzstan? Earth Surf. Process. Landforms 42, 1535–1548.
Roskosch, J., Winsemann, J., Polom, U., Brandes, C., Tsukamoto, S., Weitkamp, A., Bartholomäus, W.A., Henningsen, D., Frechen, M., 2015. Luminescence dating of ice-marginal deposits in northern Germany: evidence for repeated glaciations during the Middle Pleistocene (MIS 12 to MIS 6). Boreas 44, 103–126.
Ruegg, G.H.J., 1983. Glaciofluvial and glaciolacustrine deposits in The Netherlands. In: Ehlers, J. (Ed.), Glacial Deposits in North-West Europe. AA Balkema, Rotterdam, pp. 379–392.
Ruske, R., 1963. Zur Entstehung des Gewässernetzes in der Umgebung von Halle/Saale. Hercynia NF 1, 40–50.
Ruske, R., 1973. Stand der Erforschungen des Quartärs in den Bezirken Halle und Magdeburg. Z. Geol. Wiss. 9, 1065–1086.
Russell, A.J., Knudsen, Ó., 1999. An ice-contact rhythmite (turbidite) succession deposited during the November 1996 catastrophic outburst flood (jökulhlaup), Skeiðarárjökull, Iceland. Sediment. Geol. 127, 1–10.
Schulz, W., 1962. Gliederung der Pleistozänstratigraphie in der Umgebung von Halle (Saale). Geologie 36, 1–69.
Skupin, K., Speetzen, E., Zandstra, J.G., 1993. Die Eiszeit in Nordwestdeutschland. Zur Vereisung der Westfälischen Bucht und angrenzender Gebiete. Geologisches Landesamt Nordrhein-Westfalen, Krefeld, p. 143.
Speetzen, E., Zandstra, J.G., 2009. Elster-und Saale-Vereisung im Weser-Ems-Gebiet und ihre kristallinen Leitgeschiebegesellschaften. Münstersche Forschungen zur Geologie und Paläontologie 103, 1–113.
Stelling, G.S., 1984. On the construction of computational methods for shallow water flow problems. Rijkswaterstaat Commun. 35, 1–226.
Syme, W., 1991. Dynamically Linked Two-Dimensional/One-Dimensional Hydrodynamic Modelling Program for Rivers, Estuaries & Coastal Waters. Department of Civil Engineering, University of Queensland, p. 135. Unpublished Master Thesis.
Teller, J.T., Leverington, D.W., Mann, J.D., 2002. Freshwater outbursts to the oceans from glacial Lake Agassiz and their role in climate change during the last deglaciation. Quat. Sci. Rev. 21, 879–887.
Ter Wee, M.W., 1983. The Saalian glaciation in the northern Netherlands. In: Ehlers, J. (Ed.), Glacial Deposits in North-West Europe. AA Balkema, Rotterdam, pp. 405–412.

Thome, K.N., 1983. Gletschererosion und -akkumulation im Münsterland und angrenzenden Gebieten. Neues Jahrbuch für Geologie und Paläontologie 166, 116–138.
Toucanne, S., Zaragosi, S., Bourillet, J.F., Cremer, M., Eynaud, F., Van Vliet-Lanoë, Penaud, A., Fontanier, C., Turon, J.L., Cortijo, E., Gibbard, P.L., 2009a. Timing of massive 'Fleuve Manche' discharges over the last 350kyr: insights into the European ice-sheet oscillations and the European drainage network from MIS 10 to 2. Quat. Sci. Rev. 28, 1238–1256.
Toucanne, S., Zaragosi, S., Bourillet, J.F., Gibbard, P.L., Eynaud, F., Giraudeau, J., Turon, J.L., Cremer, M., Cortijo, E., Martinez, P., Rossignol, L., 2009b. A 1.2 Ma record of glaciation and fluvial discharge from the West European Atlantic margin. Quat. Sci. Rev. 28, 2974–2981.
TUFLOW, 2017. TUFLOW User Manual. BMT, Brisbane, p. 715.
Ullah, M.S., Bhattacharya, J.P., Dupre, W.R., 2015. Confluence scours versus incised valleys: examples from the cretaceous ferron notom delta, southeastern Utah, USA. J. Sediment. Res. 85, 445–458.
Van den Berg, M.W., Beets, D.J., 1987. Saalian glacial deposits and morphology in The Netherlands. In: van der Meer, J.J.M. (Ed.), Tills and Glaciotectonics. Balkema, Rotterdam, pp. 235–251.
Wansa, S., 1997. Die Schotterterrassen der Saale und Salza nordwestlich von Halle. Leipz. Geowiss. 5, 135–149.
Weymann, H.J., Feldmann, L., Bombien, H., 2005. Das Pleistozän des nördlichen Harzvorlands – eine Zusammenfassung. E&G - Quaternary Science Journal 55, 43–63.
Winsemann, J., Asprion, U., Meyer, T., Schramm, C., 2007. Facies characteristics of Middle Pleistocene (Saalian) ice-margin subaqueous fan and delta deposits, glacial Lake Leine, NW Germany. Sediment. Geol. 193, 105–129.
Winsemann, J., Hornung, J.J., Meinsen, J., Asprion, U., Polom, U., Brandes, C., Bußmann, M., Weber, C., 2009. Anatomy of a subaqueous ice-contact fan and delta complex, Middle Pleistocene, north-west Germany. Sedimentology 56, 1041–1076.
Winsemann, J., Brandes, C., Polom, U., 2011a. Response of a proglacial delta to rapid high-magnitude lake-level change: an integration of outcrop data and high-resolution shear-wave seismics. Basin Res. 23, 22–52.
Winsemann, J., Brandes, C., Polom, U., Weber, C., 2011b. Depositional architecture and palaeogeographic significance of Middle Pleistocene glaciolacustrine ice marginal deposits in northwestern Germany: a synoptic overview. E&G Quaternary Science Journal 60, 212–235.
Winsemann, J., Lang, J., Roskosch, J., Polom, U., Böhner, U., Brandes, C., Glotzbach, C., Frechen, M., 2015. Terrace styles and timing of terrace formation in the Weser and Leine valleys, northern Germany: response of a fluvial system to climate change and glaciation. Quat. Sci. Rev. 123, 31–57.
Winsemann, J., Alho, P., Laamanen, L., Goseberg, N., Lang, J., Klostermann, J., 2016. Flow dynamics, sedimentation and erosion of glacial lake outburst floods along the Middle Pleistocene Scandinavian Ice Sheet (northern central Europe). Boreas 45, 260–283.
Winsemann, J., Lang, J., Polom, U., Loewer, M., Igel, J., Pollok, L., Brandes, C., 2018. Ice-marginal forced regressive deltas in glacial lake basins: geomorphology, facies variability and large-scale depositional architecture. Boreas 47, 973–1002.
Woldstedt, P., 1929. Das Eiszeitalter. Enke, Stuttgart, p. 406.
Woldstedt, P., 1931. Erläuterungen zur geologischen Karte von Preussen und benachbarten deutschen Ländern, 1:25000, Blatt 3830Schöppenstedt. Preußische Geologische Landesanstalt, Berlin, p. 64.